

Summer 2013

A computational model of nanoparticle transport and delivery in tumor tissue

Vishwa Priya Podduturi

Follow this and additional works at: <https://digitalcommons.latech.edu/dissertations>

 Part of the [Biomedical Engineering and Bioengineering Commons](#)

**A COMPUTATIONAL MODEL OF NANOPARTICLE
TRANSPORT AND DELIVERY IN
TUMOR TISSUE**

by

Vishwa Priya Podduturi, M.S.

A Dissertation Presented in Partial Fulfillment
of the Requirements of the Degree
Doctor of Philosophy

COLLEGE OF ENGINEERING AND SCIENCE
LOUISIANA TECH UNIVERSITY

August, 2013

UMI Number: 3577727

All rights reserved

INFORMATION TO ALL USERS

The quality of this reproduction is dependent upon the quality of the copy submitted.

In the unlikely event that the author did not send a complete manuscript and there are missing pages, these will be noted. Also, if material had to be removed, a note will indicate the deletion.

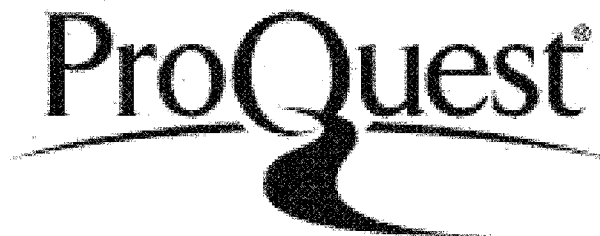


UMI 3577727

Published by ProQuest LLC 2014. Copyright in the Dissertation held by the Author.

Microform Edition © ProQuest LLC.

All rights reserved. This work is protected against unauthorized copying under Title 17, United States Code.



ProQuest LLC
789 East Eisenhower Parkway
P.O. Box 1346
Ann Arbor, MI 48106-1346

LOUISIANA TECH UNIVERSITY

THE GRADUATE SCHOOL

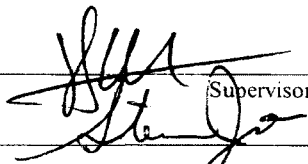
April 24, 2013

Date

We hereby recommend that the dissertation prepared under our supervision
by VISHWA PRIYA PODDUTURI

entitled A COMPUTATIONAL MODEL OF NANOPARTICLE TRANSPORT AND
DELIVERY IN TUMOR TISSUE

be accepted in partial fulfillment of the requirements for the Degree of
DOCTOR OF PHILOSOPHY IN BIOMEDICAL ENGINEERING

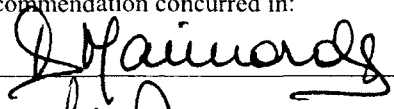


Supervisor of Dissertation Research

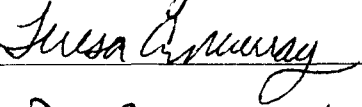

Head of Department
BIOMEDICAL ENGINEERING

Department

Recommendation concurred in:









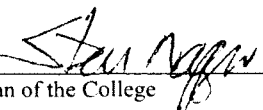
Advisory Committee

Approved: 

Director of Graduate Studies

Approved: 

Dean of the Graduate School



Dean of the College

ABSTRACT

Determining the factors that influence the delivery of nanoparticles to tumors and understanding the relative importance of each of these factors is fundamental to optimize the drug delivery process. In this research, a model that combines random walk with the pressure driven flow of nanoparticles in a tumor vasculature is modeled. Nanoparticle movement in a cylindrical tube with dimensions similar to the tumor's blood capillary with a single pore is simulated. Nanoparticle velocities are calculated as a pressure driven flow over imposed to Brownian motion. During the study, the effect of red blood cells (RBC) is also studied by comparing the delivery with and without RBC. The number and percentage of nanoparticles leaving the blood vessel through the pore is obtained as a function of pore size, nanoparticle size and concentration, interstitial pressure, and blood pressure in the tumor vasculature. The model presented here is able to determine the relative importance of these controllable parameters and thus it can be used to understand the process and predict the best conditions for nanoparticle-based treatment. When RBC are not considered, the results indicate that the nanoparticle delivery gradually increases with pore size and decreases with nanoparticle size for tumors with high interstitial fluid pressure (in this work we found this behavior for head and neck carcinoma and for metastatic melanoma with interstitial pressures of 18 mmHg and 19 mmHg, respectively). For tumors with lower interstitial fluid pressure (rectal carcinoma with 15.3 mmHg) however, delivery is about constant for almost the entire nanoparticle size

range. Though increase in nanoparticle concentration increases the number of nanoparticles being delivered, the efficiency of the delivery (percentage of nanoparticles delivered) is found to remain unaffected.

The motion of red blood cells in the capillary is also simulated and the velocity of nanoparticles between two red blood cells is obtained from the bolus flow of plasma, and the velocity between a red blood cell and the capillary wall is obtained from the lubrication theory. The results show that bolus flow of plasma in the presence of RBC pushes the NP's towards the capillary wall leading to an increased NP delivery to the tumor; however the delivery as a function of NP size, blood pressure and interstitial fluid pressure is qualitatively the same that when there are no red blood cells.

A study of nanoparticle movement through entire body is performed by considering that the nanoparticles are uniformly distributed throughout the blood circulation. The nanoparticle delivery to the tumor with time obtained from this study showed a very good to excellent agreement with the experimental results.

APPROVAL FOR SCHOLARLY DISSEMINATION

The author grants to the Prescott Memorial Library of Louisiana Tech University the right to reproduce, by appropriate methods, upon request, any or all portions of this Dissertation. It is understood that "proper request" consists of the agreement, on the part of the requesting party, that said reproduction is for his personal use and that subsequent reproduction will not occur without written approval of the author of this Dissertation. Further, any portions of the Dissertation used in books, papers, and other works must be appropriately referenced to this Dissertation.

Finally, the author of this Dissertation reserves the right to publish freely, in the literature, at any time, any or all portions of this Dissertation.

Author Vishwajit Jorjia

Date 07/30/13

DEDICATION

To my Mother

Laxmi Devi Podduturi

TABLE OF CONTENTS

ABSTRACT.....	iii
DEDICATION.....	vi
LIST OF TABLES.....	xi
LIST OF FIGURES.....	xii
ACKNOWLEDGMENTS.....	xiv
CHAPTER 1 INTRODUCTION.....	1
1.1 Goal.....	1
1.2 Rationale.....	1
1.3 Unique Physiology of Tumor Tissues.....	2
1.3.1 Angiogenesis.....	2
1.3.2 Unique Tumor Capillaries.....	4
1.3.2.1 Continuous Capillaries.....	4
1.3.2.2 Fenestrated Capillaries.....	5
1.3.2.3 Discontinuous Capillaries.....	5
1.3.3 Hypoxia.....	5
1.3.4 Interstitial Fluid Pressure.....	5
1.4 Types of Cancer.....	6
1.4.1 Carcinoma.....	6
1.4.2 Sarcoma.....	6
1.4.3 Lymphoma.....	6
1.4.4 Leukemia.....	7

1.5	Treatment Methods for Cancer	7
1.5.1	Surgery	7
1.5.2	Radiation Therapy.....	7
1.5.3	Chemotherapy	8
1.5.4	Immunotherapy	8
1.6	Nanoparticles in Cancer Treatment	8
1.6.1	Polymeric Nanoparticles.....	9
1.6.2	Liposomes	9
1.6.3	Viral Nanoparticles	10
1.6.4	Carbon Nanotubes.....	10
1.6.5	Gold Nanoparticles	10
1.7	Transport Path of Nanoparticles	11
1.7.1	Reticuloendothelial System	11
1.7.2	Circulation Half-life of Nanoparticles	12
1.7.3	Targeted Delivery to Tumor Tissue.....	12
1.7.4	Transport through Capillary Wall	13
1.7.5	Active Targeting	15
1.8	Fluid/Particle Flow Models	16
CHAPTER 2 MODEL DESCRIPTION		18
2.1	Tumor Blood Capillary	18
2.2	Nanoparticle Movement in the Capillary.....	19
2.3	Velocity of Nanoparticles	19
2.3.1	Pressure in the Capillary	20
2.3.2	Viscosity of Blood	21
2.3.3	Velocity of NP's in the Capillary.....	21

2.3.4	Velocity in the Vicinity of Pore	22
2.3.5	COMSOL Simulations	23
2.3.6	Capillary Zones	26
2.3.7	Comparison of COMSOL and Eq. 2.2 Velocities	27
2.4	Displacement Due to Collisions	29
2.5	Simulation Process and Time Step	31
2.5.1	Simulation Process	31
2.5.2	Boundary and Overlap Check	32
2.5.3	Time Step	32
2.6	Uniform Density of NP in Flow	33
CHAPTER 3 RESULTS AND DISCUSSIONS		37
3.1	Effect of NP Size in Delivery	37
3.2	Effect of Pore Diameter on Delivery	41
3.3	Comparison to an Experimental Study	42
3.4	Effect of NP Concentration in Delivery	45
3.5	Effect of Blood Pressure on the Delivery	46
CHAPTER 4 MODELLING RBC IN CAPILLARY BLOOD FLOW		48
4.1	Red Blood Cell Size and Structure	48
4.2	Hematocrit in Capillaries	48
4.3	RBC Flow in the Capillary	49
4.4	Velocity of NP's in the Capillary	50
4.4.1	Lubrication Theory	50
4.4.2	Bolus Flow	51
4.5	Results and Discussions	53
4.5.1	Comparison of NP Delivery with and without RBC	53

4.5.2 Simulations as a Function of NP Size and Blood Pressure.....	54
CHAPTER 5 NANOPARTICLE FLOW THROUGH ENTIRE BODY	58
5.1 Number of Pores on the Capillary Wall.....	58
5.2 Delivery through the Pores	59
5.3 Drug Dosage in the Blood	63
5.4 Results and Discussions.....	65
CHAPTER 6 CONCLUSIONS AND FUTURE WORK	68
6.1 Conclusions.....	68
6.2 Future Work.....	69
APPENDIX A FLOW CHART OF THE PROGRAM.....	71
A.1. Flow Chart of the Program without RBC in Capillary	72
A.2. Flow Chart of the Program with RBC in Capillary	73
APPENDIX B VBA CODE FOR COMSOL DATA	74
B.1. Subtracting Velocity of Flow with and without Pore	75
B.2. Creating Co-ordinates of Velocity Table	76
B.3. Getting Velocities for the Table from COMSOL Data.....	77
B.4. Finding the Highest Velocity in X, Y and Z Directions in Zone2	79
B.5. Comparing Velocities from Intrapolation and Table.....	80
BIBLIOGRAPHY	83

LIST OF TABLES

Table 2.1: Blood Pressure in the capillary [23],[112].....	20
Table 2.2: Values of parameters used in Eq. 2.8	31
Table 3.1: Comparison between experimental[121] and simulation results.....	44
Table 4.1: Comparison of the percentage of 100 nm NP delivered for different tumors with and without RBC in the capillary	55
Table 4.2: Percentage of NP's delivered to tumor at capillary blood pressure(CBP) 23 mmHg with and without RBC in the capillary	57
Table 5.1: Actual percentage of drugs delivered in experiments and simulations for PEG-liposomes	66
Table 5.2: Actual percentage of drugs delivered in experiments and simulations for liposomes	66

Figure 3.7: Number and percentage of NP's entering the pore as a function of volume fraction of NP in capillary	45
Figure 3.8: Percentage of NPs delivered to tumor as a function of the capillary blood pressure	46
Figure 3.9: Percentage of NPs delivered to tumor as a function of NP size for different capillary blood pressure (CBP)	47
Figure 4.1: Red Blood Cells in the Capillary Section.....	49
Figure 4.2: Velocity of NP in the thin layer.....	51
Figure 4.3: Axial velocity of the bolus flow of plasma between two RBC's [132].	52
Figure 4.4: Radial velocity of the bolus flow of plasma between RBC's [132].....	53
Figure 4.5: Comparison of NP's delivered to tumor with and without RBC in the capillary for different pore size.....	54
Figure 4.6: Percentage of NP's delivered to tumor as a function of NP size with RBC in the capillary	55
Figure 4.7: Percentage of NP's delivered to tumor as a function of capillary blood pressure in the presence of RBC in the capillary.....	56
Figure 5.1: Distribution of pores and blood pressure in the capillary at each pore	59
Figure 5.2: Schematic of the drug transport in the capillary.....	60
Figure 5.3: Delivery of NP's as a function of capillary blood pressure for 100 nm NP in head and neck carcinoma (IFP 19 mmHg)	61
Figure 5.4: NP delivered to tumor obtained from extrapolation of results in chapter 3 and 4.....	62
Figure 5.5: Delivery of NP's to tumor for different pressure gradients across the pore for 200 nm NP in rectal carcinoma (IFP 15.3 mmHg)	63
Figure 5.6: Percentage of drug dose remaining in the blood with time obtained from Ishida experiments [133]	64
Figure 5.7: Experimental and simulated results of the delivery of liposomes to the tumor	65
Figure A.1: Flow chart of the program without RBC in the capillary	72
Figure A.2: Flow chart of program with RBC in capillary.....	73

ACKNOWLEDGMENTS

I wish to express my deepest gratitude to my mentor and advisor, Dr. Pedro Derosa, for his constant advice, support and encouragement in technical and professional aspects of my research work. I would like to express my sincere thanks to my advisory committee members Dr. Patrick O'Neal, Dr. Steven A. Jones, Dr. Daniela S. Mainardi and Dr. Teresa A. Murray for their valuable advice in my research.

My special thanks are extended to Mr. Nenian Charles and Mr. Joshua S. Brown for their help in my work. I am thankful to all my group members for their support and friendship. I would like to thank my family and friends for their inspiration, continued support and encouragement. Finally, I would like to express special thanks to my husband, Siva Mahesh Tangutooru, for helping me to concentrate on completing this research and supporting me mentally.

CHAPTER 1

INTRODUCTION

1.1 Goal

The goal of this project is to develop a model that can simulate nanoparticle (NP) transport in tumor capillary and its delivery into the tumor interstitium. The role of red blood cells in the delivery of NP to the tumor is studied. The effect of NP size, capillary pore size, NP concentration, blood pressure in the tumor capillary and the interstitial pressure on the delivery of the NP's is determined.

1.2 Rationale

Cancer is a deadly disease affecting about 12.7 million people all over the world every year [1]. Cancer can be treated by surgery, radiation therapy, and chemotherapy to mention the more widespread methods. Cancer often spreads to other parts of the body and in those cases, a combination of the treatment methods mentioned above is used [2]. Surgery is an invasive procedure where the primary tumor tissue is surgically removed from the body [3]. To remove tumors spread to other parts of the body, radiation therapy or chemotherapy is used [2]. In radiation therapy, the tumor tissue is exposed to x-rays, gamma rays or charged particle radiations, thereby destroying the DNA of the cancer cells and killing the cancer tissue [4]; however, although radiation can be narrowly targeted to the desired areas, damage to surrounding healthy tissue is virtually

unavoidable. In chemotherapy, drugs introduced into the body either orally or intravenously identify the rapidly developing tumor tissue and kills it [5]. Unfortunately, the drug may also confuse rapidly dividing healthy cells of the body such as bone marrow or hair cells, with cancer cells and kill them too, leading to hair loss or more serious anemia, bleeding, and clotting problems [6]. To minimize those side effects, specific and targeted delivery is a necessity. NP's are being used as delivery vehicles to achieve this goal [7] and the drug or a radio isotope is either encapsulated in the NP or attached to it [8, 9].

NP's introduced into the body enter the blood circulation and travel through the entire body. When the NP's are in the tumor vasculature, they leave the blood circulation and enter the tumor interstitium through the capillary wall. Studying the transport of NP's through the capillary wall and understanding the effect on the delivery efficiency of the NP size, concentration, capillary pore size, blood pressure in the capillary and the interstitial pressure of the tumor, will help optimize the delivery process.

1.3 Unique Physiology of Tumor Tissues

The physiology of tumor tissue is different from normal tissue; tumor blood vessels are different from the normal blood vessels as well. Tumors develops hypoxia (lack of O₂) due to the rapid growth of tumor cells; hypoxia leads to angiogenesis [10]. Also, tumors have higher interstitial pressure than healthy tissue. These unique characteristics are discussed in detail below.

1.3.1 Angiogenesis

Due to the rapid growth and multiplication of tumor cells, more O₂ and nutrients are required and if their supply does not meet the needs of the developing tumor, the

tumor cells die. The only way to increase O_2 and nutrient delivery to tumor tissue is to increase the blood supply; the tumor does this by developing new blood vessels in a process called angiogenesis [11-14]. Angiogenesis generally also occurs in the female reproductive system, in wound healing in adults, during embryogenesis and in other diseases such as psoriasis, macular degeneration, and rheumatoid arthritis [15]. It occurs due to the increased expression of pre-angiogenic factors such as VEGF (Vascular Endothelial Growth Factor) and FGF (Fibroblast Growth Factor) [16]. Tumors are able to activate the growth factors due to local conditions such as hypoxia. Cancer cells receive a signal through the hypoxia inducible factor (HIF-1) and promote the angiogenic switch which then induces angiogenesis [17]. Tumor cells also increase FGF. Both growth factors bind to their receptors on the endothelial cell and start the activation phase of angiogenesis by activating the signal transduction pathway [11]. Activation of the endothelial cells produce Matrix metalloproteinase (MMP) which degrade the basal membrane of the blood vessels making the endothelial cells free to migrate to the angiogenic stimuli [18]. After the migration of the endothelial cells, the formation phase of angiogenesis starts where the migrated endothelial cells adhere to each other by means of E-selectin, a cell-adhesion glycoprotein. They form tube-like structures which later develop into blood capillaries [19]. Blood vessel sprouting is finally induced by binding of angiopoietin-1, which is released by Mesenchymal stem cells, with the endothelial cell receptors [20, 21]. Mesenchymal cells differentiate into pericytes to form an outer layer for the new blood vessel [15].

1.3.2 Unique Tumor Capillaries

The blood capillaries in tumor differ from the blood capillaries of the normal organs in the body [10]. The normal blood capillaries are called continuous capillaries whereas the blood capillaries in tumor are the discontinuous blood capillaries [22]. The basic structure of capillaries and different types of blood capillaries are explained in detail below.

Blood Capillaries are the vessels where the true exchange of gas and nutrients between the blood and the interstitial fluid (fluid present in the tissues) occur. O₂ carried by the red blood cells and the nutrients in the blood plasma like glucose, vitamins, fatty acids and amino acids, are transported to the tissues through the capillaries. CO₂, metabolic waste and excess nutrients, water, and minerals in the tissues are transported back through the capillaries and lymphatic system. The diameter of the capillaries is in the range of 5-10 um [23]. The entire exchange occurs through the capillary wall which is formed by glycocalyx, endothelium, and basement membrane [24]. The glycoproteins, with a negative charge, form the glycocalyx [25], and it is surrounded by the endothelial cells which form a single cell tube. The endothelial cells are bounded by the junctional proteins and are covered by the basement membrane which is an electron dense fiber matrix layer [22] that consists of laminin, type IV collagen, fibronectin, proteoglycan, and glycoproteins [26].

1.3.2.1 Continuous Capillaries

Endothelial cells of the continuous capillaries are bound together by junctional proteins. Occasionally some of the proteins are missed at the junctions forming pores in the capillary wall [22].

1.3.2.2 Fenestrated Capillaries

Endothelial cells of fenestrated capillaries contain fenestrae which are openings in the cells. Some of the fenestrae completely open into the tissue whereas the others are covered by the basement membrane [27]. The open fenestrae can transport larger molecules into the tissues. Fenestrated capillaries are present in the liver and kidneys where the filtration occurs [22].

1.3.2.3 Discontinuous Capillaries

Discontinuous capillaries occur in newly formed blood vessels through angiogenesis [11]. The endothelial cells have larger gaps and the basement membrane is also discontinuous, allowing the transport of larger molecules [22].

1.3.3 Hypoxia

Hypoxia is the reduced availability of O_2 . According to the mechanism observed from the studies of Thomlinson and Gray [28], due to the rapid growth and division of tumor cells, the new cells occupy the space which is far away from the existing blood vessel and hence do not get enough O_2 supply and finally become hypoxic. An alternate mechanism called the acute hypoxia model which states that the hypoxia occurs due to the fluctuating blood flow to the tumor has also been proposed.

1.3.4 Interstitial Fluid Pressure

Interstitial fluid is the fluid present in tissues which surrounds the cells. The interstitial pressure in tumor tissues is high compared to normal tissues due to the abnormal tumor blood vessels and lymph vessels [29, 30]. Due to larger pores, the tumor blood vessels are leaky and hence allow the flow of proteins and other molecules from the vessel into the tumor thereby increasing the colloidal osmotic pressure in the tumor.

Lymph vessels play an effective role in maintaining the interstitial pressure in normal tissues by absorbing the interstitial fluid but they are non-functional or absent in the tumor tissues [31-33]. Due to the poor lymphatic system in tumors, the interstitial fluid and the proteins remain in the tumor increasing the interstitial fluid pressure.

1.4 Types of Cancer

Cancer develops in many organs of the human body and also in bones. Cancer is basically differentiated into four types: Carcinoma, Sarcoma, Lymphoma and Leukemia [34].

1.4.1 Carcinoma

Carcinoma is the most common type of cancer arising from epithelial cells which cover the inner and outer surface of all body organs [35, 36]. The most common carcinomas are the lung cancer, breast cancer, skin cancer, and colon cancer [34].

1.4.2 Sarcoma

Sarcoma is a less common type of cancer arising from bone or soft tissues like muscles, fat, nerves, blood vessels etc [37]. Osteosarcoma (bone), liposarcoma (fat), leiomyosarcoma (smooth muscle), neurofibrosarcoma (nerves), synovial sarcoma (Joints), angiosarcoma (blood vessels) are some of the sarcomas affecting the body [38].

1.4.3 Lymphoma

Lymphoma arises from lymphocytes (a type of white blood cells) which form the body's immune system [39]. Lymphocytes are present in the lymph system comprising of lymph nodes, thymus gland, spleen and liver [40].

1.4.4 Leukemia

Leukemia affects the blood-forming cells, mostly white blood forming-cells. It develops in bone marrow and enters the blood. From the blood, it spreads to the central nervous system, liver, spleen and other body parts [41].

1.5 Treatment Methods for Cancer

Cancer can be treated through surgery, radiation, chemotherapy and immunotherapy [42-44]. A combination of these methods is used based on the type, location, and severity of the cancer.

1.5.1 Surgery

Surgery is generally done to remove the cancer tissue from the body. If cancer develops in a particular tissue and spreads to other parts of the body, surgery is used to remove the primary source of the cancer, and chemotherapy or radiation therapy is used to treat the cancer spread to the other parts of the body [45]. Surgery is an invasive procedure in which the surgeon cuts into the body to access the tumor tissue. Less invasive alternatives such as laparoscopy can also be used, in this procedure, the surgeon inserts a small camera and surgical tools into the body by making small incisions [46]. Through the camera, the surgeon is able to visualize the tissue and perform surgery. Patient recovery time is also shorter for this kind of surgery.

1.5.2 Radiation Therapy

In radiation therapy, the tumor tissue is exposed to x- rays, gamma- rays or ionic particles to damage the DNA of the tumor cells [47]. A cell needs DNA to divide and multiply in number, once the DNA is damaged; the cell cannot divide and eventually dies. The source of the radiation can come from outside or can be introduced into the

body. In the external beam radiation, the source of the radiation is a machine such as linear accelerator or a cobalt radiotherapy unit. For internal radiation therapy (also called as brachytherapy), radioactive materials are introduced into the body [48]. The radioactive materials are encapsulated in small particles and placed in the tumor tissue or near it.

1.5.3 Chemotherapy

In chemotherapy, a drug (chemical) which has the ability to kill cancer cells is introduced into the body either orally or intravenously. Paclitaxel and Doxorubicin are two of the drugs used in chemotherapy [49]. When the drug is introduced into the body, it identifies rapidly dividing cells of the body and kills them. The drug may also confuse the rapidly dividing healthy cells of the body, such as bone marrow or hair cells, with the tumor tissue. Thus the drug kills those healthy cells leading to anemia [50], bleeding and clotting problems and hair loss [6].

1.5.4 Immunotherapy

In immunotherapy, the body's immune system is activated such that it destroys the cancer cells [51]. Cancer vaccines, antibodies, and certain types of cells, such as T-cells, dendrite cells and natural killer cells, are being used to activate the immune system against cancer in the body [52].

1.6 Nanoparticles in Cancer Treatment

In radiation therapy, radiation targeting the tumor tissue may hit the neighboring healthy cells and damage them [53]. Even in chemotherapy, the drug kills healthy cells, as mentioned earlier. To reduce damage to the healthy cells of the body, the drug used in chemotherapy or the radioisotope used in the radiation therapy need to be targeted

efficiently to the tumor cells. NP's are used in cancer treatment as delivery vehicles to help in achieving a specific and targeted delivery [54]. These NP's are made of gold, liposomes, polymers, viral NP's, etc [55]. Gold nanoshells and nanorods have unique optical properties that allow for non-invasive, real-time monitoring of NP concentration in the blood [56]. Most of these NP's are currently only used in research or are in clinical trials.

1.6.1 Polymeric Nanoparticles

Chitosan, albumin and heparin are naturally occurring polymers used in drug delivery. Albumin is used as a carrier where paclitaxel (albumin-bound paclitaxel is called abraxane) is bound to it and introduced into the body to treat metastatic breast cancer [57]. Synthetic polymers such as N-(2-hydroxypropyl)-methacrylamide copolymer (HPMA), polystyrene-maleic anhydride copolymer, polyethylene glycol (PEG), and poly-L-glutamic acid (PGA) are also used as drug carriers [58]. Polymeric micelles are other type of polymeric NP's whose inner region is hydrophobic and are used to store the drug. The outer region is hydrophilic, allowing the NP to travel through the blood circulation [59]. Dendrimers are another type of polymeric NP's made of synthetic polymers and have a central core region and many branched monomers coming out of the core. The surface functionality of dendrimers can be easily modified to obtain a targeted drug delivery [60].

1.6.2 Liposomes

Liposomes are the most commonly used NP's for drug delivery and are made of lipids [61]. They are closed colloidal structures where the outer layer, made of a lipid bilayer, can hold hydrophobic drugs and the aqueous inner layer can hold the hydrophilic

drugs [62, 63]. Doxil and Myocet are some of the liposome based NP's which are approved for metastatic breast cancer treatment [64, 65]. Stealth liposomes formed by coating liposomes with poly-ethylene glycol (PEG) improve the efficiency of the liposome NP's by increasing their circulation time in the human body [66].

1.6.3 Viral Nanoparticles

Viruses such as cowpea virus and cowpea chlorotic mottle virus have been developed to use as drug carriers [62]. They are developed from plant, animal, or insect viruses [67]. Viral NP's can also be used for cancer imaging [68].

1.6.4 Carbon Nanotubes

Carbon nanotubes are being studied as drug delivery vehicles. Carbon nanotubes are insoluble and hence are toxic to the body [62], but they can be made soluble and less toxic by functionalizing them with proteins, bio active peptides etc. to change their chemical properties [69].

1.6.5 Gold Nanoparticles

Gold NP's are used as photo thermal therapy agents which kill the cancer cells by heating them [70]. Tumor cells cannot withstand heat as well as the normal cells, due to the poor blood supply, and hence they are killed [71]. This effect is maximized as metal nanoparticles in the tumor enhance the heat absorption. In photo thermal therapy, light is used to heat the tissue. Gold NP's are used as photo thermal therapy agents because of their surface plasma resonance. By varying the composition and the dimensions of the gold NP's, the surface plasma resonance in the range from the visible to the near infrared region can be achieved [72]. When the near infrared light is focused on the gold NP's, the electron start exhibiting resonance, forming a heated electron gas

[73]. This heat is dissipated into the surrounding tissue, thus heating the cells [71]. So, by delivering gold NP's into the tumor tissue and focusing light on the body externally, tumor cells can be heated and killed. Gold NP's of different shapes such as nanospheres, nanorods, nanoshells and nanocages are used [70].

1.7 Transport Path of Nanoparticles

NP's are introduced into the body either orally or intravenously. Once they are in the body, they enter the blood circulation and travel throughout the body. Within the body, the reticuloendothelial system (RES) tries to remove them from the circulation [74].

1.7.1 Reticuloendothelial System

The reticuloendothelial system is part of the immune system and includes phagocytic cells, such as liver kupffer cells, the spleen, macrophages, monocytes, and lymphatic vessels [75]. The phagocytic cells engulf foreign substances, such as bacteria and viruses, and render them incapable of attacking the body. Monocytes are the phagocytic cells derived from bone marrow stem cells and exist in the blood stream. Monocytes which leave the circulation and enter other tissues of body, such as liver, spleen, and lymph nodes are called as macrophages [76]. The liver has most of the macrophages of the body which are called kupffer cells [77]. When NP's travel along the circulatory system, monocytes identify them as foreign substances and engulf them thereby removing them from circulation. These engulfed NP's are accumulated in the liver or spleen [75].

1.7.2 Circulation Half-life of Nanoparticles

The time in which the NP's concentration in the blood circulation becomes half its initial concentration is defined as the circulation half time of the NP's [78]. NP's removed from the circulation accumulate either in tumor tissue or in liver and spleen. The circulation half-life of the NP's also depend on the formation of NP aggregates (nanoparticle clusters). If NP's have a strong attraction between them, they tend to attach to one another and form aggregates which are removed from the circulation and accumulated in liver or spleen, thereby decreasing the circulation half-life of NP's [79, 80].

1.7.3 Targeted Delivery to Tumor Tissue

NP's travel the entire body through the blood circulation and enter the blood vessels of various tissues. For targeted delivery, NP's should leave the blood vessel and enter the tissue only when it is in the tumor blood vessel, by utilizing the leakiness of tumor tissue blood vessels. The pore size in the capillary walls of tumor blood vessels is in the range of 200-800 nm whereas the pore size in the capillary walls of normal tissue is in the range of 7-9 nm [22, 81, 82]. NP's bigger than the pore size of normal blood vessels and smaller than the pore size of tumor blood vessels will leak mostly into the tumor tissues resulting in maximum drug delivery to the tumor. Figure 1.1 shows the schematic of the targeted delivery of NP's into tumor tissue.

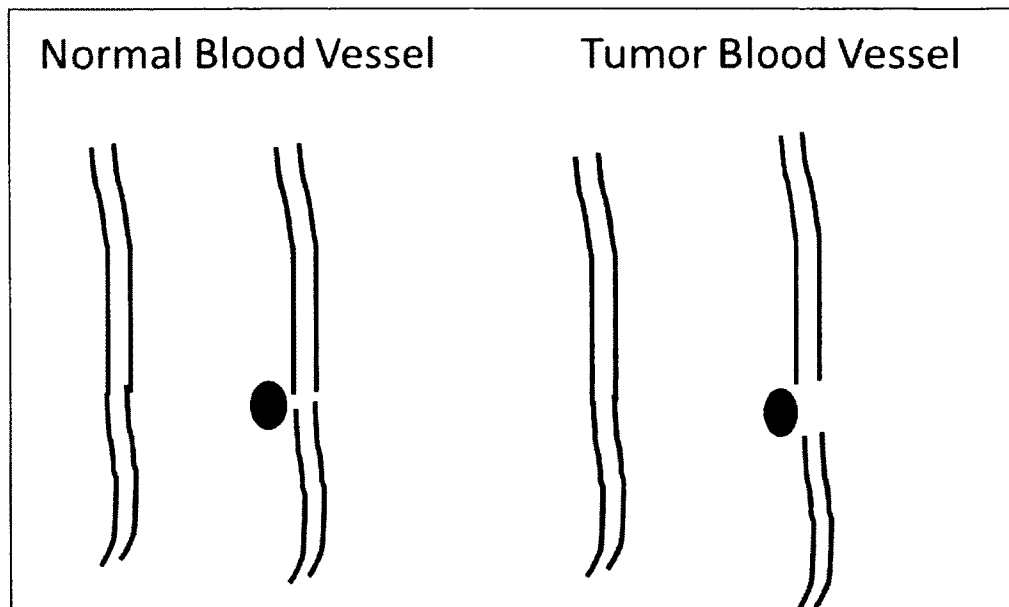


Figure 1.1: Schematic showing a NP in normal blood vessel and tumor blood vessel

The left figure shows a NP in the blood vessel and the capillary wall of a normal tissue with small pores whereas the right figure shows a NP in the blood vessel and the capillary wall of a tumor tissue with large pores.

1.7.4 Transport through Capillary Wall

Endothelial cells form the major part of the capillary wall. The membrane of the endothelial cells, which is made of lipid bilayers, is permeable to O_2 , CO_2 and other lipid soluble solutes such as fatty acids, cholesterol and phospholipids [83, 84]. The endothelial cells are tightly packed to each other and the cell junctions form channels called intercellular clefts that are 7-9 nm wide [22, 23]. The intercellular clefts allow transport of water, small hydrophilic solutes, such as glucose, urea, lactic acid and small ions such as Na^+ , K^+ , Cl^- , through this channels [85-87].

A special means of transport, called transcytosis, enables the transport of some plasma proteins such as albumin [88]. The endothelial cells engulf the proteins through

endocytosis and transport them to the other side of the cell by vesicles, which are small membrane-enclosed sacs [89, 90]. The protein is finally released into the interstitium of tissue through exocytosis. Most of the time, transcytosis allows transport of specific macromolecules due to receptor-based transport [91]. Endothelial surfaces have receptors for certain macromolecules, such as albumin, transferrin, insulin and ceruloplasmin [92-95]. When these molecules are present in a blood capillary, their receptors on the endothelial surface activate the process of transcytosis.

NP's used for drug delivery are larger compared to the intercellular clefts, and hence they cannot pass through them. But, as stated in an earlier section, tumor capillaries have large pores between the endothelial cells making them leakier and the major transport of NP's across the tumor capillary walls is due to convection of NP's through these large pores [96]. Convection arises due to the pressure gradient across the pore and due to the large size of NP's, convection is dominant over diffusion [97].

NP's can transport across the capillary wall through transcytosis by coupling them with the molecules that can activate the receptor-based transcytosis [98, 99]. However, if a NP transport through transcytosis, specific delivery to the target tissue becomes difficult because transcytosis also occurs across the healthy tissue capillary wall leading to significant amount of NP delivered to the healthy cells which is undesirable [98]. To achieve specific delivery in this case, NP's are coupled with the superparamagnetic iron oxide NP's (SPIONs) and an external magnetic field is applied which directs the NP to the desired location [100]. Transcytosis of NP's is generally used in delivering drugs to tissues which have a tightly bound endothelial cell barrier in their capillary walls (for example, brain) [98].

1.7.5 Active Targeting

Once NP's cross the capillary wall and enter the tumor tissue, they travel through the tumor interstitium to reach the cells [101]. The tumor interstitium consists of the interstitial fluid, collagen matrix and tumor cells [102]. Transport of NP's in the tumor interstitium is through diffusion and convection. Diffusion arises due to the concentration gradient of the NP's within the tumor interstitium whereas convection is due to the change in the interstitial fluid pressure in the tumor interstitium [103]. Convection occurs at the tumor periphery since the interstitial pressure gradient only exists at the periphery. At the interior of the tumor, the interstitial pressure is almost constant [101].

The NP's moving in the tumor interstitium should be able to identify the tumor cell and release drugs to kill them; that can be achieved by active targeting. The NP carrying drug is coupled with a ligand, which is tumor specific, so when the NP travels through the tumor interstitium and comes near to a tumor cell, the ligand recognizes the tumor cell, binds to it and releases the drug. Antibodies are widely used as targeting ligands [104]. As an example, NP's conjugated with monoclonal antibodies (mAb) increased the uptake of that nanoparticle by six times. Nucleic acid aptamers [105] and peptide ligands [106] are also used as targeting agents.

In summary, the transport path of the NP's includes transport through the blood circulation, across the capillary wall and through the interstitium. A detailed study of the transport of NP's through this system and the factors which can affect the transport can help increase the drug dosage delivered to the target tissue.

1.8 Fluid/Particle Flow Models

Pozrikids and Farrow developed a model to study the fluid flow in a tumor tissue in which Poiseuille's law gives the flow rate of fluid moving through a cylindrical tube. Starling's equation gives the net fluid movement through the capillary wall due to hydrostatic and osmotic pressure difference between the tumor and the capillary and Darcy's law gives the flow through the tumor interstitium [22, 107]. These authors computed the hydraulic conductivities for a wide range of tissue and capillary wall conductivities.

Soltani and Chen developed a numerical model to study the fluid flow in the tumor interstitium that assumes the tumor tissue to be spherical in shape and conservation of mass and momentum is used in the simulation of fluid flow [108]. In this model, the tumor interstitium is classified into three regions based on the blood supply. (1) The well vascularized region at the periphery of the tumor interstitium, which is very close to the tumor blood vessels; (2) the semi-necrotic region, which has a reduced blood supply because the region is farther from the blood vessels; and (3) the core of the interstitium, which is necrotic region due to a poor blood supply. The authors studied the interstitial fluid pressure as a function of the area of the necrotic region in the tumor and found that with an increase in the necrotic radius, the maximum pressure inside the tumor decreases.

Chang et al., developed a network model to study the delivery of colloidal drugs where the tumor interstitium was represented by a 2-D square network model and the movement of colloidal particles in the interstitium was a result of the hemodynamic forces, the gravitational force, the van der Waals attraction, and the electrostatic

repulsion interaction forces, and the random forces caused by the Brownian motion behavior of micro-particles [109]. The authors studied the drug delivery for different drug concentrations and found that the concentration of drug particles in the tumor decreases with a decrease in blood velocity in the arterial vasculature. They also found that an increase in the tumor interstitial pressure causes a slow increase in the concentration of drug in the tumor whereas an increase in the arterial pressure results in a fast increase in the concentration of drug in the tumor.

There are certain limitations in the above mentioned models, the blood is assumed to be a Newtonian fluid in the models where blood in real behaves as a Non-Newtonian fluid [22]. Also the main focus of the Soltani and Chen models was the transport through the tumor interstitium and the transport through the capillary is not studied. Although Pozrikids studied the transport through the capillary wall, the study was basically on the fluid flow through it.

In study presented in this dissertation, the transport of the NP's in a capillary and their delivery to a tumor interstitial through the capillary wall is simulated. The effect of various parameters such as the NP size, pore size (pores on the capillary wall), NP concentration, blood pressure, and interstitial pressure on the NP delivery through the capillary wall is determined. The effect of the explicit presence of red blood cell is determined in this work to only affect the quantity but not the delivery profile. The ultimate aim of this work is to determine effect of these parameters on the NP delivery, once these are known, favorable conditions for NP delivery can be derived which will eventually result in an increased delivery to the tumor tissues.

CHAPTER 2

MODEL DESCRIPTION

2.1 Tumor Blood Capillary

Nanoparticle's (NP's) entering the blood circulatory system travel through arteries, arterioles, capillaries, venules, and veins but it is only at the capillaries that they enter the tissue leaving the blood circulation. Hence the movement of NP's in the capillaries is simulated. A section of blood capillary is built as a single cylindrical tube with a diameter of 8 μm [23], a length of 10 μm , and with a single pore of diameter in the 100-600 nm range representing a pore present in the capillary wall. Figure 2.1 shows the segment of a capillary with a single pore in its wall simulated in MATLAB [110].

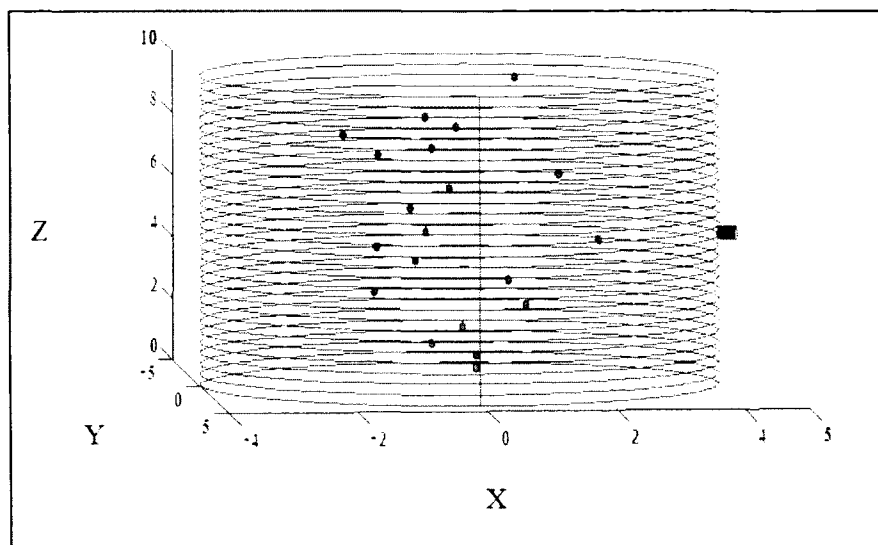


Figure 2.1: Segment of capillary with a single pore with NP's.

2.2 Nanoparticle Movement in the Capillary

In this model, NP's are assumed to move along with the blood flowing through the capillary and hence have the velocity of blood (which is given in Section 2.3.3). The movement of NP's in the capillary occurs primarily due to their velocity and secondarily due to their collisions with other molecules in the blood, which is simulated as Brownian motion. Brownian motion in general is the random motion of a particle due to its collisions with other particles [111].

2.3 Velocity of Nanoparticles

The velocity of blood depends mainly on two factors:

1. The pressure gradient present along the length of the capillary
2. The viscosity of blood.

2.3.1 Pressure in the Capillary

A capillary arises from an arteriole and terminates into a venule. There exists a pressure difference between the arterial and the venous end of the capillary. Figure 2.2 shows the structure of a capillary with its two ends and Table 2.1 shows the normal blood pressure at the ends of the capillary in human body.

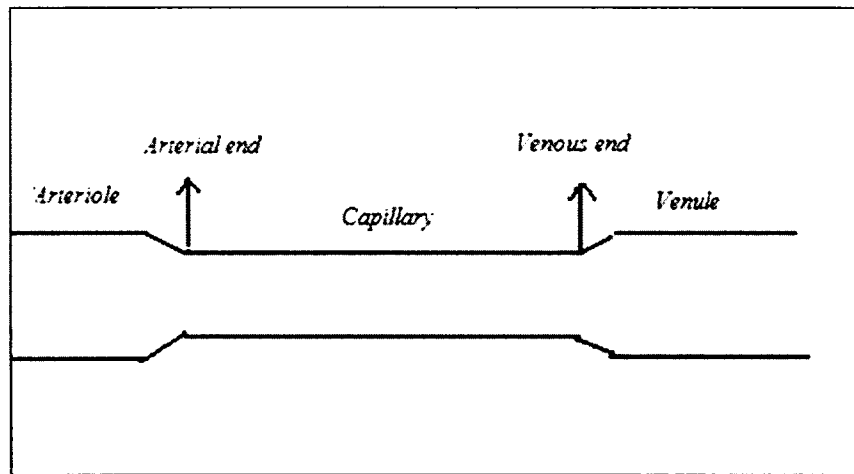


Figure 2.2: Capillary with arterial and venous ends

Table 2.1: Blood Pressure in the capillary [23],[112]

Parameters	Values
Pressure at arterial end of capillary	30 mmHg
Pressure at venous end of capillary	10 mmHg
Length of the whole capillary	700 μm
Pressure gradient along the capillary	0.0286 mmHg / μm

When the blood pressure is increased or decreased in the model, the pressure values are different from the values shown in Table 2.1.

2.3.2 Viscosity of Blood

Blood consists of plasma and cells. The major component of plasma is water. It also consists of plasma proteins, such as albumin and globulin. About 55 % of the blood volume is plasma and the rest is cells [113]. Due to the presence of cells, blood behaves as a Non-Newtonian fluid whose viscosity is not constant, unlike a Newtonian fluid [114]. For blood, apparent viscosity decreases with an increased stress which makes it a shear thinning fluid [115].

Viscosity of blood is calculated from a power law. The apparent viscosity of a power law fluid is a function of shear rate raised to a power [22]. Eq. 2.1 shows the apparent viscosity of a power law fluid.

$$\eta_{app} = k|\dot{\gamma}_x|^{n-1}. \quad \text{Eq. 2.1}$$

Where, η_{app} is the apparent viscosity, $\dot{\gamma}_x$ is the shear rate, k and n are the quantities which depend on the fluid. If $n = 1$, the fluid is Newtonian. If $n < 1$, it is a shear thinning fluid and if $n > 1$, the fluid is shear thickening. Since the Non-Newtonian nature of the blood is due to the presence of red blood cells in it, the value of n and k also depend on the number of cells present in the blood (called as hematocrit). The values of n and k used in this model are 0.708 and 17 mPa. secⁿ, respectively [116].

2.3.3 Velocity of NP's in the Capillary

Blood flow in the capillary is laminar. Velocity of a pressure-driven flow of a power law fluid in a cylindrical tube is obtained from Eq. 2.2 [22]. As already mentioned, the capillary is assumed as a cylindrical tube and blood, which is a power law fluid, flows due to the pressure difference in the capillary, Eq. 2.2 can be used to obtain the velocity of the blood in capillaries.

$$V_z = \left(\frac{\nabla_z P}{2 \times k} \right)^{\frac{1}{n}} \times \left(\frac{n}{n+1} \right) \times \left(R^{\frac{n+1}{n}} - r^{\frac{n+1}{n}} \right). \quad \text{Eq. 2.2}$$

Where V_z is the velocity of blood along the length of the capillary, $\nabla_z P$ is the pressure gradient along the length of the capillary, R is the radius of the capillary and r is the distance from the center of the capillary.

Since velocity of NP is assumed to be equal to the velocity of blood (as already mentioned), Eq. 2.2 gives the velocity of NP's in the capillary. The velocity profile of the NP's obtained from Eq. 2.2 is shown in Figure 2.3.

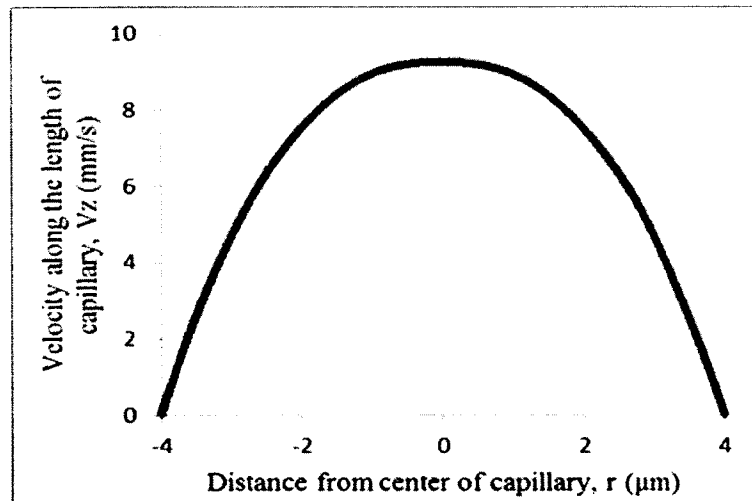


Figure 2.3: Velocity profile of the blood obtained from Eq. 2.2

Velocity of NP's is maximum at the center and decreases as they move away from the center and becomes zero at the capillary walls.

2.3.4 Velocity in the Vicinity of Pore

The pressure in the tumor interstitium is different from the pressure inside the blood capillary which leads to a pressure gradient through the pore. Figure 2.4 shows the pressure gradients in a capillary in the vicinity of the pore and away from the pore.

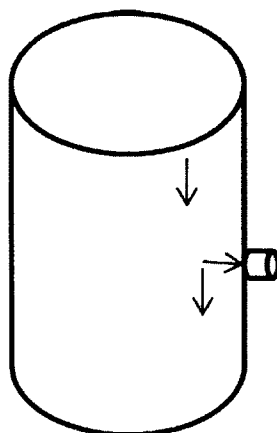


Figure 2.4: Pressure gradients acting in the capillary

It can be seen from Figure 2.4 that there is an added component of pressure gradient in the direction of the pore in its vicinity. Eq. 2.2 is only applicable to a fully developed flow in a cylindrical tube where velocity only exists along the length of the capillary and hence is not applicable in the vicinity of the pore. COMSOL is an alternative to get the velocity near the pore [117].

2.3.5 COMSOL Simulations

COMSOL MULTIPHYSICS is a finite element analysis based simulation software which is used for various engineering and physics applications [118]. Laminar flow of blood in the capillary is simulated in COMSOL using the Navier-Stokes equations which are derived by applying Newton's second law of motion to fluid flow. The equation also assumes that the fluid stress is due to the viscosity of the fluid and the pressure acting on it. Blood is modeled as an incompressible fluid where density remains constant even when the pressure and the temperature vary [22]. Density of blood in this simulation is 1060 kg/m^3 [119] and the viscosity of blood is obtained from the power law parameters mentioned in Section 2.3.2.

The mesh size used in these simulations is $0.4\ \mu\text{m}$. A section of capillary with a single pore simulated in COMSOL is shown in Figure 2.5

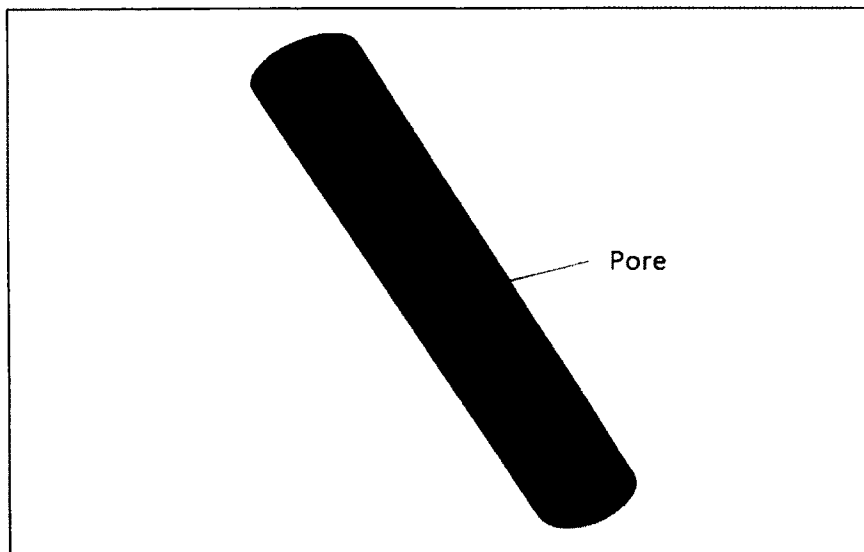


Figure 2.5: Capillary with single pore simulated in COMSOL 4.0a

To find the effect of pore on the velocity of NP's, a capillary with a pore and without one are simulated. Velocities obtained from one simulation are subtracted from the other to get the velocity of a NP due to the pore. Figure 2.6, Figure 2.7 and Figure 2.8 show the peak velocities in the X, Y and Z directions in the capillary near the pore.

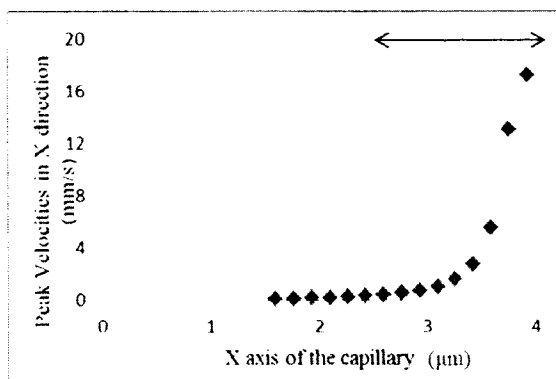


Figure 2.6: Velocity in X direction of the capillary due to the pore

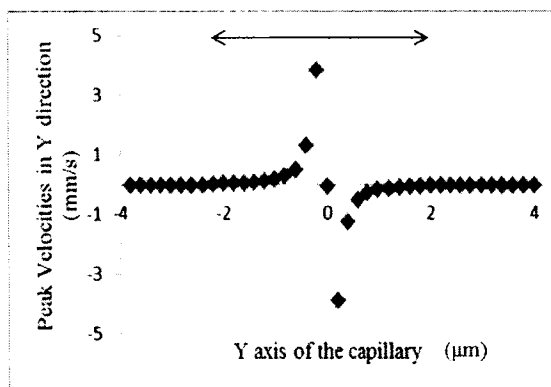


Figure 2.7: Velocity in Y direction of the capillary due to the pore

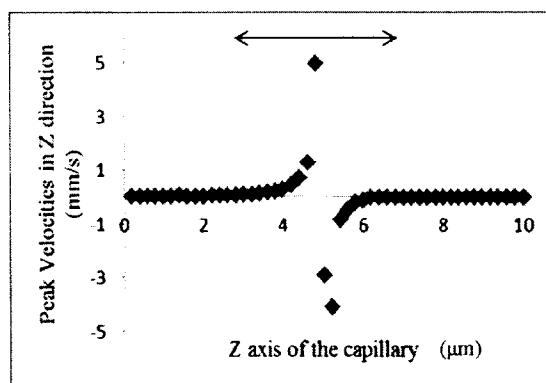


Figure 2.8: Velocity in Z direction of capillary near the pore

The capillary blood pressure, the tumor interstitial fluid pressure (IFP) and the pore diameter in these figures are 20 mmHg, 15.3 mmHg and 400 nm, respectively. The pore location is at (4,0,5). It can be seen from the figures that the velocity is higher near the pore and decreases as the NPs move away from the pore. The horizontal line shows the area where the effect of the pore is present and prominent.

2.3.6 Capillary Zones

It is observed from the figures that the effect of the pore on the velocity of the nanoparticle is present only in a certain area near the pore. In the rest of the capillary, the effect of the pore is not prominent or even negligible. Hence, the capillary is divided into two zones (Figure 2.9):

1. Zone 1: Area in the capillary where the effect of the pore is not present.
2. Zone 2: Area in the capillary where the effect of the pore is present.

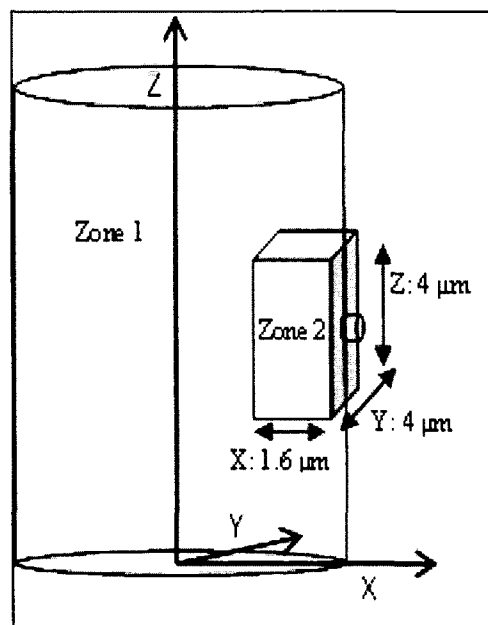


Figure 2.9: Zone 1 and 2 of the capillary

The dimensions of zone 2 are obtained from the positions of the double headed solid lines in Figure 2.6, Figure 2.7 and Figure 2.8. The velocity of NP in zone 1 is obtained from Eq. 2.2. Since in zone 2 the pressure gradients has two components (one parallel to the axis of the cylinder and the other towards the pore) as shown in Figure 2.4, velocity due to the component of the pressure gradient along the length of the capillary is obtained from Eq. 2.2 and velocity due to the component of the pressure gradient along the pore is obtained from COMSOL. These two velocities add up to give the resultant velocity of NP in zone 2.

2.3.7 Comparison of COMSOL and Eq. 2.2 Velocities

As described above, the velocity profile for the particles leaving the capillary through the pore is obtained from COMSOL simulations, but the velocity profile in the capillary comes from Eq. 2.2. In order to ensure consistency, a comparison was made between the velocity obtained from Eq. 2.2 and COMSOL. A cylindrical tube without a pore is simulated in COMSOL and the velocity profile obtained is plotted along with the velocity profile of Eq. 2.2, as shown in Figure 2.10.

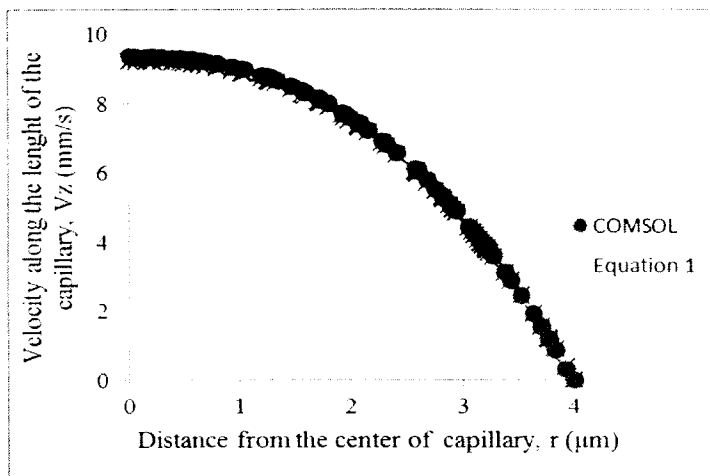


Figure 2.10: Velocity in the capillary obtained from COMSOL and Eq. 2.2.

From Figure 2.10, it can be seen that the velocities from COMSOL and Eq. 2.2 overlap with each other showing that they are in good agreement with each other. To make a more in detailed comparison, % difference between both the velocities is plotted in Figure 2.11.

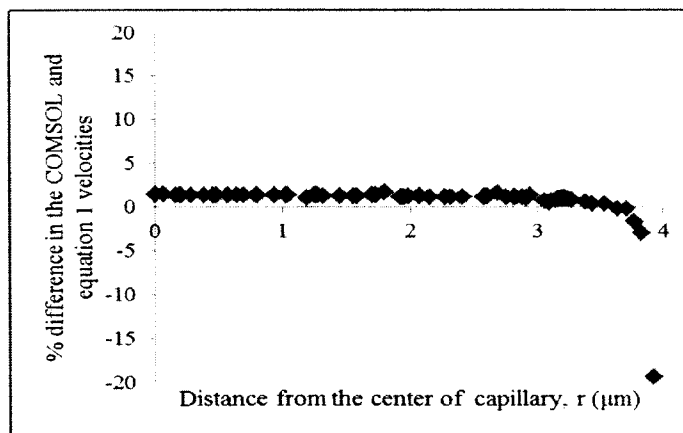


Figure 2.11: Percentage difference between the COMSOL and Eq. 2.2 velocity.

It can be seen that the difference is small throughout the tube except near the wall. The difference is 2% or less up to a distance of 3.85 μm from the center of the capillary.

For a distance above $3.85 \mu\text{m}$ ($0.15 \mu\text{m}$ or less from the wall) the % difference is above 5%, however notice that in this region the velocity is small thus the relative error is expected to be large. nevertheless COMSOL results will be used near the pore where the velocity is not small. Since the velocity from COMSOL and Eq. 2.2 are close to each other, it is concluded that obtaining the velocities from COMSOL near the pore will lead to no significant error.

2.4 Displacement Due to Collisions

The NP in the blood undergoes collisions with other molecules which add momentum to it thereby displacing it. Collisions occur in any random direction and hence Brownian motion is modeled as a random walk.

The displacement due to one collision is derived in this section. Since water is a major component of blood, the model considers collisions between the NP and the water molecule and assumes that water molecule transfers all its momentum to the NP.

$$\vec{P}_{Na} = \vec{P}_{Nb} + \vec{P}_w. \quad \text{Eq. 2.3}$$

Where \vec{P}_{Na} and \vec{P}_{Nb} are respectively the linear momentum of the NP after and before the collision and \vec{P}_w is the linear momentum of a single water molecule. As the Brownian motion will be over-imposed to the displacement due to the blood flow, the common drift velocity on the NP and the water can be subtracted and assume the NP is initially at rest. Thus,

$$M\vec{V}_{Na} = m\vec{V}_w. \quad \text{Eq. 2.4}$$

M and m are the mass of the NP and the water molecule respectively, \vec{V}_{Na} is the velocity of the NP after collision and \vec{V}_w is the velocity of the water molecule. So, after the collision

$$\vec{V}_{Na} = \frac{m \vec{V}_w}{M}. \quad \text{Eq. 2.5}$$

Since water molecules move due to thermal energy,

$$\frac{3}{2} K_B T = \frac{1}{2} m V_w^2. \quad \text{Eq. 2.6}$$

K_B is the Boltzmann Constant and T is the temperature.

Solving Eq. 2.6 for V_w and using it in Eq. 2.5,

$$V_{Na} = \frac{\sqrt{3 K_B T m}}{M}. \quad \text{Eq. 2.7}$$

Then the maximum distance D_{max} will be

$$D_{max} = \frac{\sqrt{3 K_B T m}}{\rho V_{NP}} \tau. \quad \text{Eq. 2.8}$$

Where τ is the time step of the simulation and the NP's mass was written in terms of its density

$$M = \rho V_{NP}. \quad \text{Eq. 2.9}$$

Where ρ is the density of the NP and V_{NP} is the volume of the NP. Table 2.2 shows the values used in the Eq. 2.8.

Table 2.2: Values of parameters used in Eq. 2.8

Parameters	Values
Mass of one water molecule	$2.99 \text{ e}^{-26} \text{ Kg}$
Boltzmann Constant	$1.380648 \text{ e}^{-23} \text{ JK}^{-1}$
Body Temperature	310 K
Time step	4 μs

The component of the displacement due to the over-imposed Brownian motion is calculated by randomly selecting a hopping distance from zero to a maximum and randomly selecting the inclination and azimuth angles between zero and π and zero and 2π respectively where the maximum displacement is the displacement due to one collision which is given by Eq. 2.8. A NP may actually undergo more than one collision in a single time step, but the displacement due to each collision may be in a different direction leading, in average, to a smaller overall displacement and thus the actual displacement is determined randomly between zero and D_{max} .

2.5 Simulation Process and Time Step

2.5.1 Simulation Process

The simulation process is as follows:

1. NP's are initially distributed randomly inside the cylinder
2. NP's are selected one by one and the zone in which they are present is identified. A new position is determined as the time step times the velocity of the particle.
3. From this point, the particle is displaced due to the Brownian motion.

4. If the particle enters the pore, it is accounted as delivered, and another particle is added to the volume to keep the density constant
5. If the particle leaves the cylinder at the bottom, another particle is inserted at the top

2.5.2 Boundary and Overlap Check

Every time the NP is displaced, a boundary check and overlap check is performed. Boundary check is done to verify that the NP does not cross the boundaries of the capillary except at the two outlets (pore and the end of the capillary). If the NP crossed the boundary, then the NP is again displaced from the current position assuming that it hit the capillary wall and bounced back. Overlap check is done to verify that the NP does not overlap with another NP in the capillary. If overlap occurs, the NP is displaced again assuming a collision.

2.5.3 Time Step

The criterion to select the time step is that no particle is allowed to move from its current position a distance larger than its own radius in one time step. Limiting the maximum hop distance is necessary because overlap is only checked at the initial and final positions, so if the hop distance is too large, a particle may find itself, after the hop, at the other side of a NP in its way without ever overlapping, leading to an unphysical behavior. Choosing the radius and not the diameter as the maximum distance is an extra safety measure as particles will not always be on a direct head-on collision.

Given that NP's velocity in zone 2 may be significantly larger than in zone 1, as the maximum velocity in zone 2 depends on the difference between the capillary blood pressure and the IFP, a different (shorter) time step is chosen for this zone. The time is

chosen to be a factor of the time steps in zone 1 such that particles still will not move a distance larger than their radius in one time step. Having two different time steps for zone 1 and zone 2 optimizes simulation time as the time step necessary for zone 2 is unnecessarily short for particles in zone 1. The timeline of particles in both regions is maintained in sync by allowing particles in zone 2 to move a number of times equal to the factor between the two time steps for each time particles in zone 1 are moved.

2.6 Uniform Density of NP in Flow

To maintain a continuous flow of NP in the capillary, a new NP is added as soon as another NP leaves the capillary. To maintain a uniform density of NP in the capillary, the capillary is divided into concentric sections as shown in Figure 2.12 and the NP is entered into these sections based on a probability.

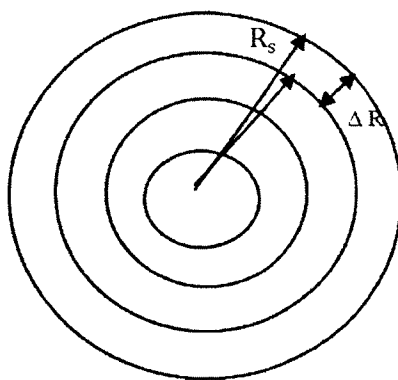


Figure 2.12: Cross section of the capillary showing its division into sections each of thickness 10 nm

The probability of the NP entering a segment is derived as shown below. The number of NP's entering a section is proportional to the velocity of the nanoparticles in the segment (from Eq. 2.2) and the volume of the section. Within the ring of the section, NP's are randomly placed. The concentration of NP in a section is given by Eq. 2.10

$$\rho = \frac{M \times N}{Vol}. \quad \text{Eq. 2.10}$$

ρ is the concentration of NP in a section. M is the Mass of the NP, N is the number of NP present in the section, Vol is the volume of the section. The volume of the section is obtained as

$$Vol = \pi(R_s^2 - (R_s - \Delta R)^2) \times H. \quad \text{Eq. 2.11}$$

R_s is the outer radius of section, ΔR is the thickness of the section and H is the length of the capillary section in the simulation. Simplifying Eq. 2.11, we get

$$Vol = \pi H(2R_s \Delta R - \Delta R^2). \quad \text{Eq. 2.12}$$

Substituting Eq. 2.12 in Eq. 2.10 and re-arranging, the number of NP in a segment is

$$N = \frac{\rho \pi H(2R_s \Delta R - \Delta R^2)}{M}. \quad \text{Eq. 2.13}$$

The NP concentration in the section, the length of the sections, and the mass of the NP, remains constant throughout the simulations. Hence,

$$N \propto 2R_s \Delta R - \Delta R^2. \quad \text{Eq. 2.14}$$

The number of NP entering a segment should be proportional to the number of NP required in the segment to maintain a uniform density throughout the capillary

$$N_e \propto N. \quad \text{Eq. 2.15}$$

N_e is the number of NP entering each section. From Eq. 2.14 and Eq. 2.15,

$$N_e \propto 2R_s \Delta R - \Delta R^2. \quad \text{Eq. 2.16}$$

In a given amount of time, the number of NPs entering each section N_e should also be equal to the number of NPs leaving that section in the same amount of time N_l . As the length of all sections is the same, the number of NPs leaving a particular section is proportional to the NP's speed in that section.

$$N_l = N_e \propto V_z. \quad \text{Eq. 2.17}$$

From Eq. 2.16 and Eq. 2.17,

$$N_e \propto (2R_s \Delta R - \Delta R^2) V_z. \quad \text{Eq. 2.18}$$

Hence, probability of NP entering a section is

$$p = \frac{(2R_s \Delta R - \Delta R^2) V_z}{\sum_{i=1}^n (2R_{s_i} \Delta R - \Delta R^2) V_{z_i}}. \quad \text{Eq. 2.19}$$

Where n is the number of sections.

Simulations were performed to check if the probability derived in Eq. 2.19 gives a uniform distribution of NP's in the capillary. Figure 2.13 shows the density of NPs in the sections of the capillary for NP diameter 200 nm.

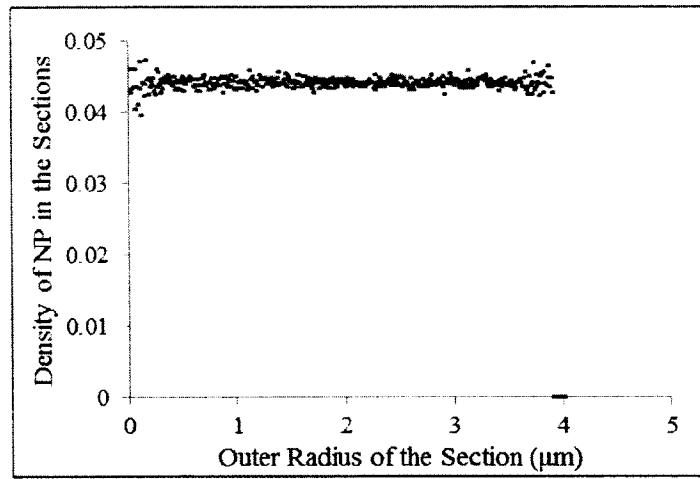


Figure 2.13: Density of NP's in the sections of capillary

It is obvious from Figure 2.13 that the densities are constant in all sections of outer radius less than 3.9 μm and for the remaining sections, the density is zero. This is because the center of the NP is considered as its position and a NP of radius 0.1 μm present in a section of radius above 3.9 μm will be crossing the boundaries of the capillary which is not physically possible. Hence, NP's are not allowed to enter those

sections which are named as zero density zones. This plot proves that a uniform distribution of NPs in the capillary is achieved with probability equation derived.

CHAPTER 3

RESULTS AND DISCUSSIONS

3.1 Effect of NP Size in Delivery

Simulations are performed to study the delivery of NP's as a function of their size. The pore diameter and the capillary blood pressure at the pore are 400 nm and 20 mmHg in these calculations. The simulations are performed on tumors with different interstitial fluid pressure (IFP), head and neck carcinoma (19 mmHg), metastatic melanoma (18 mmHg), and rectal carcinoma (15.3 mmHg)[120]. Hypothetical tumors with a pressure of 17 mmHg and 16 mmHg are also simulated to complete the set. Number of NPs delivered to the tumor as a function of NP size for tumors with different IFP is plotted as Figure 3.1. All the simulations are run for five trails. The average of the delivery results obtained from the five trials gives the actual delivery and the standard deviation of the delivery rates obtained for these five trials gives the error bars of these simulations.

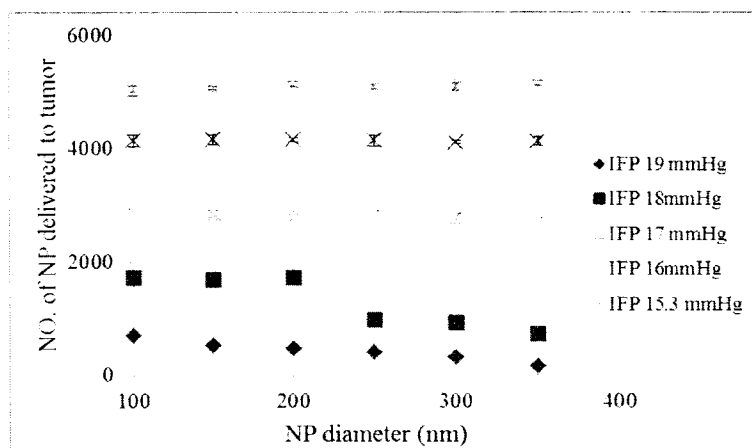


Figure 3.1: Number of NP's entering the tumor as a function of NP size

It can be seen from Figure 3.1 that the delivery of NP's to the tumor decreases with an increase in NP size for tumors of IFP 19 and 18 mmHg. A particle can be dragged into the pore or continue its way through the capillary, as the particle size increases, the chances of missing the pore also increases as depicted in Figure 3.2.

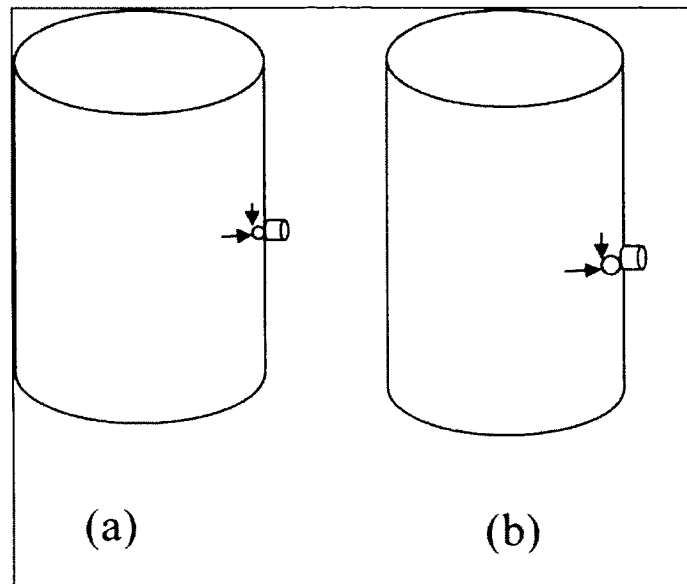


Figure 3.2: (a) Arrows denote the pressures acting on the NP near the pore. (b) A larger NP hitting the capillary wall and missing the pore

As IFP decreases, the pressure gradient between the blood capillary and the interstitium increases and with that the drag forces on the NPs also increase. For IFP of 17mmHg, the effect of particle size is significantly smaller than for 18 mmHg and 19 mmHg, and for 16 mmHg and 15.3 mmHg, the effect is virtually negligible. Figure 3.3 shows the percent of NPs delivered for the same simulations mentioned in the previous paragraph.

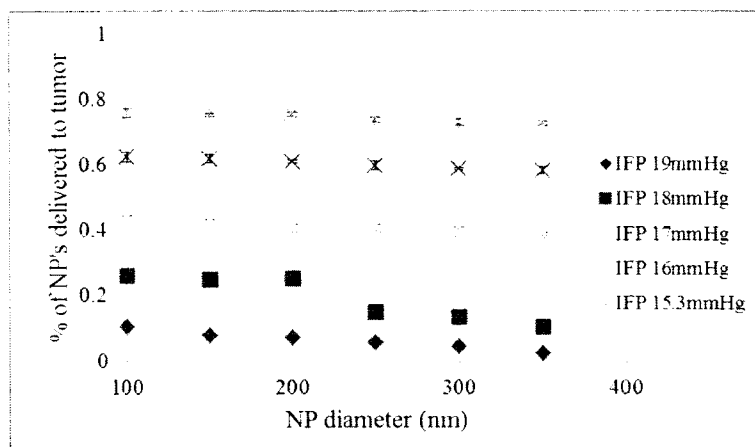


Figure 3.3: Percent of NPs entering the tumor as a function of NP size

Comparison of Figure 3.1 and Figure 3.3 shows that percentage of NPs delivered decreases slightly with particle size for IFP 16 and 15.3 mmHg where as the number of NPs delivered increases for the same IFP. This behavior can be explained with the help of Figure 3.4

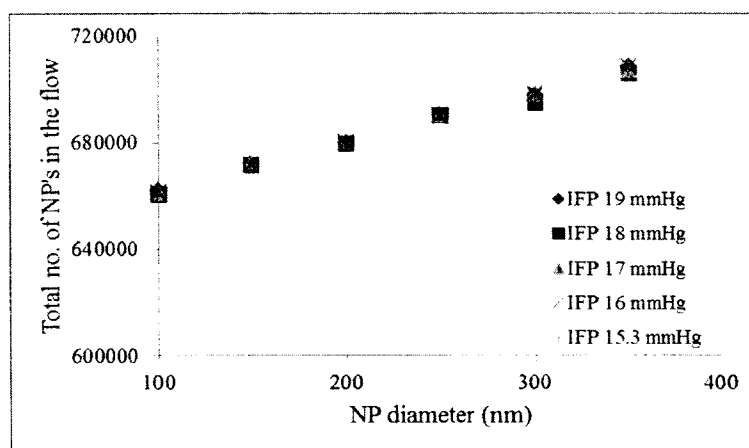


Figure 3.4: Total number of NPs in the blood flow

The total number of NP's in the flow in a given time period increases as the size of NP's increases as shown in Figure 3.4 this is because for larger NP's, the zero density

zone near the wall is larger (particles need to be at least 1 radius away from the wall), hence, as the NP size increases, the NPs that are the closest to the wall (this is the group from where most of the particles delivered to the tumor come from) are farther away than for smaller ones and they are dragged with the blood flow at a higher velocity. So NPs are added more often and more NPs can miss the pore as they move faster. This is not an artifact of the simulation, in a real experiment [121], larger particles will also move faster near the capillary wall than their smaller counterparts as they will be exposed to faster moving blood.

3.2 Effect of Pore Diameter on Delivery

NP delivery as a function of pore diameter is simulated for NP of size 200 nm and capillary blood pressure 20 mmHg. Simulations for head and neck carcinoma, metastatic melanoma and rectal carcinoma are performed. The results are shown in Figure 3.5

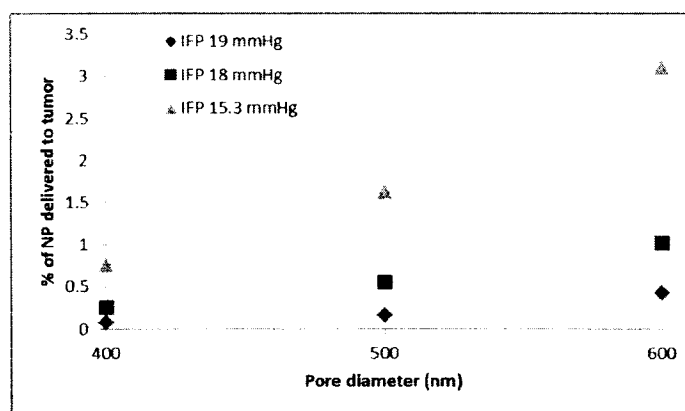


Figure 3.5: Percent of NPs entering pore as a function of pore size

The results from Figure 3.5 indicate that the NP delivery increases with the pore diameter for all three tumors. Unlike the case previously studied, where for low IFP, the delivery is almost independent of the particle size; such an effect is not observed here.

Clearly the relative NP-pore size is not the only factor in the delivery, the difference is that when the pore size is fixed, the relative size (pore-NP) changes but all NP experience the same drag force. However, changing the pore size changes the relative size but also changes the fluid velocity, thus further affecting NP delivery.

3.3 Comparison to an Experimental Study

NP delivery to tumors is studied in a way that can be directly compared to the experimental results. Experiments were performed by G. Kong [121] by introducing NPs of different sizes into the body of mice with tumors. Later, the tumor tissue was heated and the experiment was repeated. NPs of diameter 100, 200 and 400 nm were used in the experiment. Delivery of albumin was also monitored. The experimentalists observed a decrease in the delivery with an increase in the NP size at both temperatures, in agreement with the results presented here in previous sections, with an increased delivery of all NP sizes for the higher temperature. The explanation given was that heat increases the pore size leading to an increase in the number of NPs delivered.

Considering that all the pores in the vessel are of the same size is not a good assumption, thus to compare the results from our model to the experimental results mentioned above, an analysis was made by studying the delivery to a tumor assuming a distribution of pore sizes rather than a single size. For that, simulations were conducted for three different pore sizes and the results were averaged with a Gaussian-distributed weight. Two distributions of pore sizes centered at different values were simulated. The first distribution has pores of size 40 nm, 100 nm and 160 nm. The mean pore size is 100 nm and the standard deviation is 60 nm. The second distribution has pores of size 340 nm, 400 nm and 460 nm. The mean pore is 400 nm and the standard deviation is also 60

nm. The reason for choosing the above pore sizes is because the tumor vasculature used in the experiment seems to have a cut-off pore size of 100 nm before heating [121]. After heating, the experimentalists reported a cut-off pore size greater than 400 nm [121]. NP's of the same size as studied in the experiment are used here. Capillary blood pressure and the tumor IFP in this simulation are 20 and 18 mmHg, respectively. Figure 3.6 shows the results obtained from the experiments [121] and simulations.

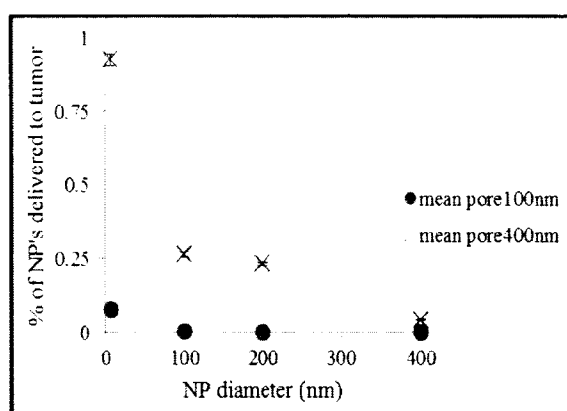


Figure 3.6: NP delivery to a tumor considering a Gaussian distribution of pore size.

As seen in Figure 3.6, for the mean pore diameter of 100 nm, NP of 200 and 400 nm do not enter the pore at all since the pore is smaller than them. There is a marginal delivery of 100 nm NP because the distribution of the pore size includes a 160 nm pore which allows some of the 100 nm NP through it. The delivery of 7 nm albumin is the largest because it is smaller than all the pores. For the mean pore diameter of 400 nm, the delivery of all the NP's increased. Table 3.1 shows the simulation results compared to the experiment.

Table 3.1: Comparison between experimental[121] and simulation results

Nanoparticles Compared	Experiments	Simulations
100 nm NP - Albumin (cut-off pore size 100 nm)	-95%	-99%
200 nm NP-100 nm NP (cut-off pore size > 400 nm)	-37%	-12%
200 nm NP-400 nm NP (cut-off pore size > 400 nm)	-53%	-82%

In the experiments, for a cut-off pore size of 100 nm, the decrease in the delivery of 100 nm NP compared with the delivery of albumin is 95%. In the simulations, for the mean pore diameter of 100 nm, a 99 % decrease in the delivery of 100 nm NP as compared to the albumin is observed. For the higher temperature experiment, NP delivery is observed to decrease 37% as the NP size increase from 100 nm to 200 nm, and 53% as the NP size increases from 200 nm to 400 nm. The results obtained from the simulations, for a mean pore diameter of 400 nm show a decrease of 12% as the NP size increases from 100 nm to 200 nm, and 82% as the NP size increases from 200 nm to 400 nm. A difference between the experimental and the simulation results exists because the exact experimental conditions are not known (i.e. the tumor IFP is not reported in the experiments). As already mentioned (Figure 3.3), the effect of NP size on the delivery varies with the tumor IFP. Also, the exact pore size in the capillary is not known. A cut-off pore size > 400 nm in the experiments may also include pores larger than 460 nm and hence might have resulted in a larger delivery of 400 nm NP than in the simulations. It is worth noticing that the experimental results have large error bars and the percentages reported above are within the experimental error except for the 400 nm NP and albumin. The delivery of albumin in the experiments and the simulations is observed to be

different. We believe that this is due to the fact that the albumin can also transport through the vesicles in the capillary walls by means of transcytosis [122]. Since the simulations consider delivery through the pores alone, while other mechanisms are available in the experiment, there is no hope to get albumin delivery right. This is not a problem for NPs.

3.4 Effect of NP Concentration in Delivery

Delivery as a function of NP concentration in blood is simulated for a NP diameter of 200 nm, pore diameter of 400 nm, and capillary blood pressure of 20 mmHg. Simulations are performed for head and neck carcinoma, metastatic melanoma, and rectal carcinoma. Results are shown in Figure 3.7.

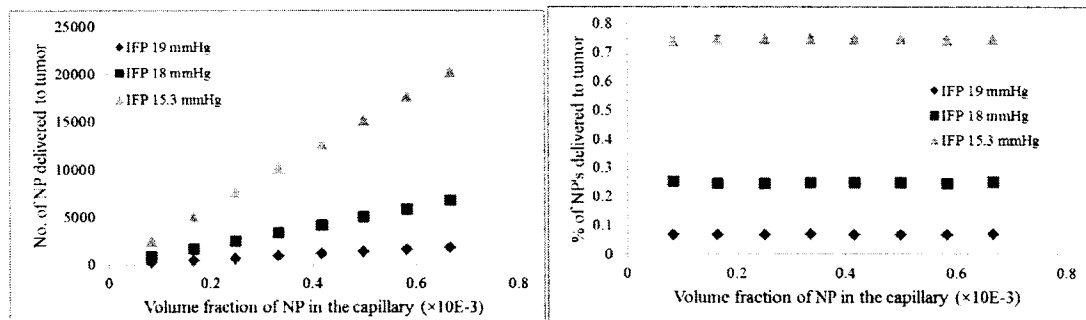


Figure 3.7: Number and percentage of NP's entering the pore as a function of volume fraction of NP in capillary

The results indicate that the number of NPs entering the pore increases with an increase in the NP concentration, but the percentage of NPs entering the tumor does not improve much for all the tumors. From the results, it can be stated that the increase in the NP concentration does not improve the efficiency of delivery through a pore at a given time, but due to the increased concentration, NPs are available in the blood for a longer time and, hence, they are available for more cycles of the blood around the body, thereby

increasing the tumor uptake over time. However this will also increase the uptake by healthy tissues and organs like the liver. This imposes a tradeoff that has to be decided on each particular case.

3.5 Effect of Blood Pressure on the Delivery

NP delivery as a function of blood pressure in the capillary is simulated for NP and a pore diameter of 200 nm and 400 nm, respectively. Simulations are performed for all three tumors. Capillary blood pressure at the pore is increased from 20 to 23 mmHg in steps of 1 mmHg keeping the tumor IFP constant. Figure 3.8 shows the percent of NPs delivered.

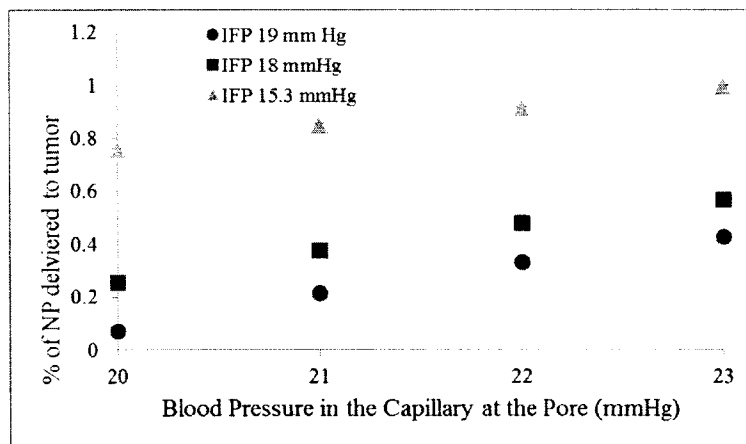


Figure 3.8: Percentage of NPs delivered to tumor as a function of the capillary blood pressure

The results indicate that the delivery of NP's to the tumor increases linearly with an increase in the blood pressure for all the three tumors. Due to the increase in the blood pressure, the difference in the pressure across the capillary wall also increases, leading to an increase in the velocity towards the pore, and thereby pulling more NP into it.

The delivery of NPs to the tumor as a function of their diameter for different capillary blood pressure (CBP) is simulated. The pore diameter and the IFP in this case are 400 nm and 19 mmHg, respectively. Results are shown in Figure 3.9.

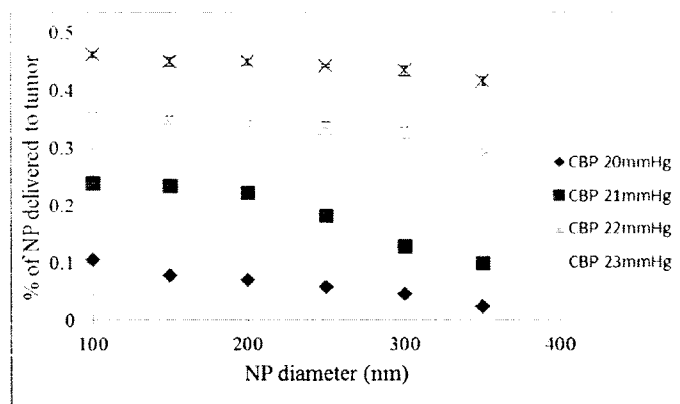


Figure 3.9: Percentage of NPs delivered to tumor as a function of NP size for different capillary blood pressure (CBP)

Delivery follows a similar trend as shown in Figure 3.3, as the capillary blood pressure increases, for a constant IFP delivery of NPs to the tumor becomes less sensitive to their size. Putting together the results from Figure 3.3 and Figure 3.9, it can be stated that as the pressure gradient across the pore increases, either due to an increase in the capillary blood pressure or due to a decrease in the tumor IFP, the effect of NP size on their delivery to the tumor becomes less significant.

CHAPTER 4

MODELLING RBC IN CAPILLARY BLOOD FLOW

4.1 Red Blood Cell Size and Structure

Red Blood Cells (RBC's) are biconcave discs with diameters in the 7-8 μm range, a thickness of 2.5 μm at the edges, and 1 μm at the center [123]. The surface topology of RBC can be modeled from Eq. 4.1[124].

$$z = 0.5\sqrt{1 - (x^2 + y^2)} (a_0 + a_1(x^2 + y^2) + a_2(x^4 + y^4)). \quad \text{Eq. 4.1}$$

where $-1 \leq x \leq 1$; $-1 \leq y \leq 1$; $a_0 = 0.207$, $a_1 = 2.002$, $a_2 = -1.122$; x , y and z are dimensionless parameters scaled as X/R , Y/R and Z/R ; X , Y , Z are the Cartesian coordinates representing RBC surface and R is the radius of the RBC.

4.2 Hematocrit in Capillaries

Hematocrit is the physiological parameter which gives the volume fraction of RBC's present in the blood volume. Hematocrit in large blood vessels (arteries and veins) is in the range of 30-55%, whereas in the capillaries, it drops to 10-20% [123]. Hematocrit for a single RBC in the capillary section is calculated from Eq. 4.2.

$$\text{Hematocrit} = \frac{\text{Volume of single RBC}}{\text{Volume of capillary section}} \times 100. \quad \text{Eq. 4.2}$$

The volume of a single RBC is $9.0 \times 10^{-17} \text{m}^3$ [125]. The radius and height of the capillary section are 4 μm and 10 μm , respectively, and hence the volume of the capillary

section is $5.03 \times 10^{-16} \text{ m}^3$. Substituting both the volumes in Eq. 4.2 gives a hematocrit of 18%, which is within the physiological range [123]. In this model, the NP flow in the RBC containing the capillary is studied and since a capillary section of length $10 \text{ }\mu\text{m}$ contains one RBC, a capillary section of length $20 \text{ }\mu\text{m}$ is simulated with two RBC's in it. Figure 4.1 shows the capillary section with two RBC's.

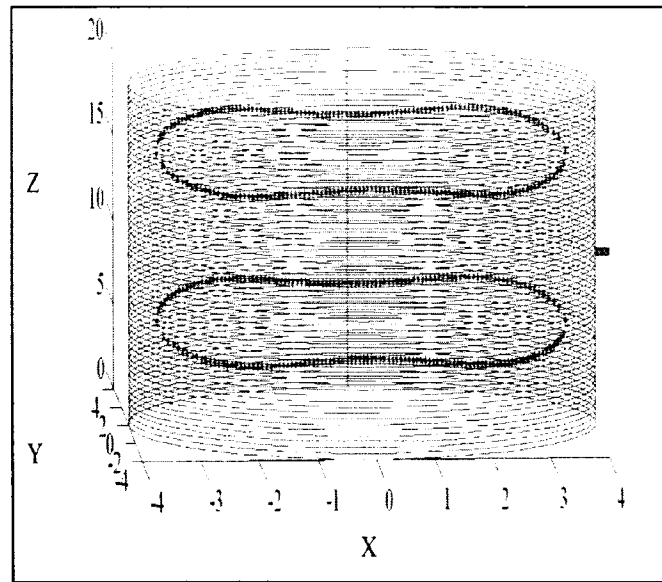


Figure 4.1: Red Blood Cells in the Capillary Section

4.3 RBC Flow in the Capillary

Only one RBC (diameter $7 \text{ }\mu\text{m}$) can enter a capillary (diameter $8 \text{ }\mu\text{m}$) at a time leading to a single file flow of RBC's in the capillary. Also, RBC's in the capillary tend to be at the center and align along the axis of the capillary, leading to a higher RBC velocity than the mean velocity of the blood flow [126]. Albrecht and his group [127] conducted some experiments to study the ratio of the velocity of RBC to the mean velocity of the blood plasma in capillaries with diameters in the range of $3.3\text{-}11.0 \text{ }\mu\text{m}$. According to their results, the ratio between the velocity of the RBC and the average

velocity of the blood plasma is 1.43 for a capillary of diameter 8 μm . Since the mean velocity of the blood is half its maximum velocity in the capillary [22] , utilizing the results of the above experimental group gives the velocity of RBC in the capillary.

4.4 Velocity of NP's in the Capillary

A thin layer of plasma flow exists in between the RBC and the capillary wall where the plasma lubricates the flow of RBC and the velocity of the NP in this layer is obtained from lubrication theory [128], whereas the velocity of NP's between two RBC's is called the bolus flow [129].

4.4.1 Lubrication Theory

Lubrication theory generally gives the flow of a thin layer of fluid between two surfaces. The lubrication theory equation is shown in Eq. 4.3 [130].

$$\frac{\partial^2 v_1}{\partial^2 a} = \frac{1}{\eta} \frac{dP}{dz} ; 0 < a < w. \quad \text{Eq. 4.3}$$

where v_1 is the velocity of the plasma (and NP's) in the thin layer, a is the distance from the RBC surface to the capillary wall in the thin layer, w is the width of the thin layer (difference between the capillary radius and the RBC radius gives the width of the thin layer), η is the viscosity of the plasma (0.0035 Pa.s [131]), and $\frac{dP}{dz}$ is the pressure gradient along the capillary. Integrating Eq. 4.3 twice gives

$$v_1 = \frac{1}{2\eta} \frac{dP}{dz} a^2 + c_1 a + c_2. \quad \text{Eq. 4.4}$$

C_1 and C_2 are the integration constants. The boundary conditions are given from Eq. 4.5 and Eq. 4.6 where V_{rbc} is the velocity of the RBC.

$$\text{At the surface of RBC,} \quad a = 0; v_1 = v_{\text{rbc}}. \quad \text{Eq. 4.5}$$

$$\text{At the capillary wall,} \quad a = w; v_1 = 0. \quad \text{Eq. 4.6}$$

Applying boundary conditions to Eq. 4.4, we get

$$v_1 = \frac{1}{2\eta} \frac{dP}{dz} (a^2 - wa) + \frac{v_{rbc}}{w} (w - a). \quad \text{Eq. 4.7}$$

Figure 4.2 shows the velocity of the NP in the thin layer obtained from Eq. 4.7.

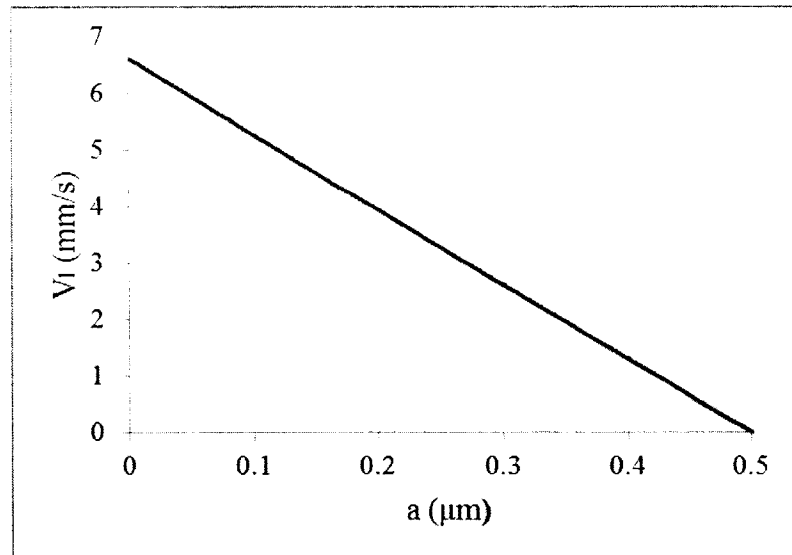


Figure 4.2: Velocity of NP in the thin layer

Figure 4.2 shows that as the NP moves from the surface of the RBC to the wall, its velocity decreases linearly and finally becomes zero at the wall.

4.4.2 Bolus Flow

Plasma in the capillary gets trapped between the RBC's forming eddies around them; this flow is called the bolus flow. The velocity of the bolus flow of the plasma is obtained from the work done by Y. C. Fung [132]. Figure 4.3 gives the axial velocity of the bolus flow of the plasma.

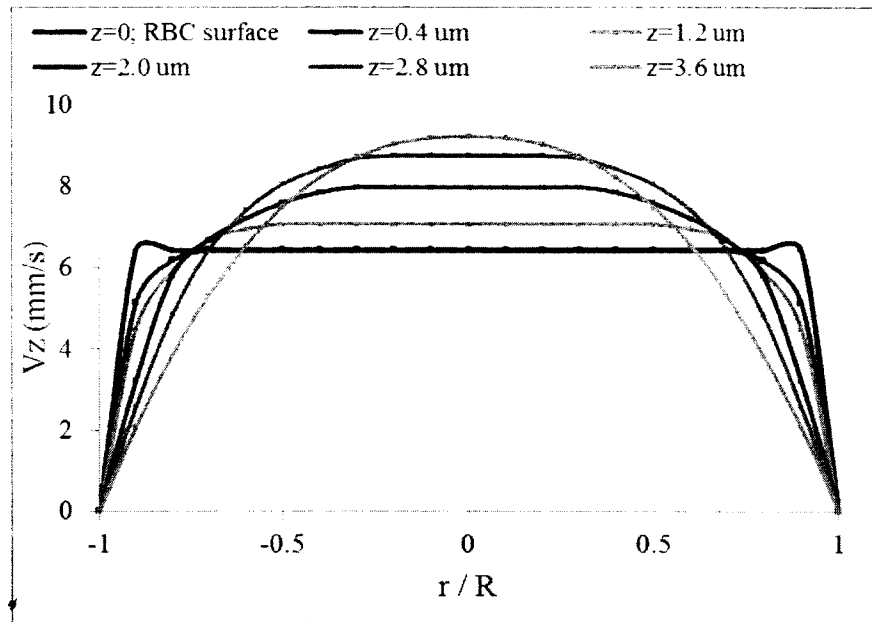


Figure 4.3: Axial velocity of the bolus flow of plasma between two RBC's [132]

The axial velocity of the plasma at a distance of above $3.6 \mu\text{m}$ from the RBC's surface is near parabolic and is the same as the velocity profile used in Chapter 3 where RBC's are not explicitly included in the model. As the plasma gets closer to the RBC's surface, the axial velocity of the plasma decreases and the velocity profile becomes blunt at the center. At the surface of the RBC, velocity of plasma is equal to the RBC's velocity until the radial distance from the center is equal to the RBC's radius, i.e., $-0.9 \leq r/R \leq 0.9$ and for rest of the capillary (the beginning of the thin layer), the velocity linearly drops to zero, which shows that the bolus flow follows the lubrication theory at the RBC's surface. Figure 4.4 shows the radial velocity of the bolus flow of the plasma.

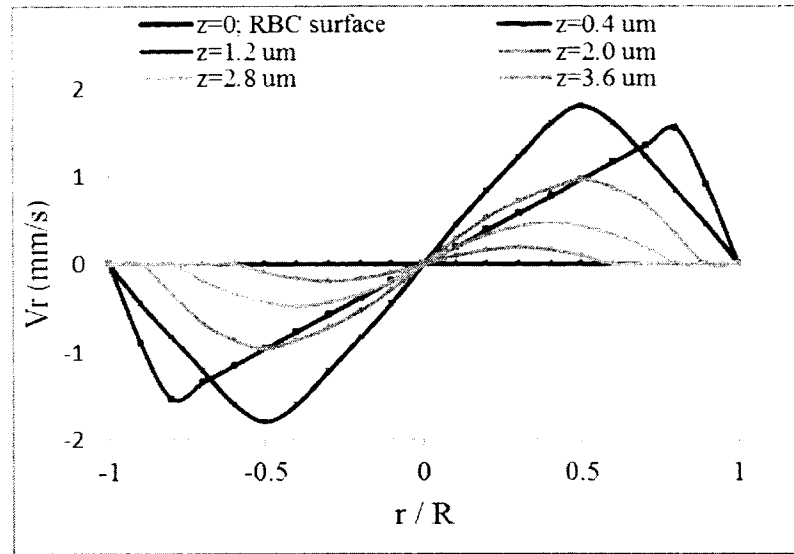


Figure 4.4: Radial velocity of the bolus flow of plasma between RBC's [132]

Figure 4.4 shows that the radial velocity is maximum when the plasma is at a distance of 1.2 μm from the RBC's surface and the velocity decreases as the plasma moves nearer to the RBC's surface or farther to it. At the RBC's surface, radial velocity is zero. The most important feature of this profile is that the velocity is directed towards the capillary wall and hence a lateral movement of NP's in the plasma towards the capillary wall is expected.

4.5 Results and Discussions

4.5.1 Comparison of NP Delivery with and without RBC

Simulations were conducted to study the impact of RBC on the NP delivery to the tumor and the results obtained were compared to the NP delivery without RBC in the capillary. Figure 4.5 shows the NP delivery to head and neck carcinoma (IFP 19 mmHg) for different pore diameters.

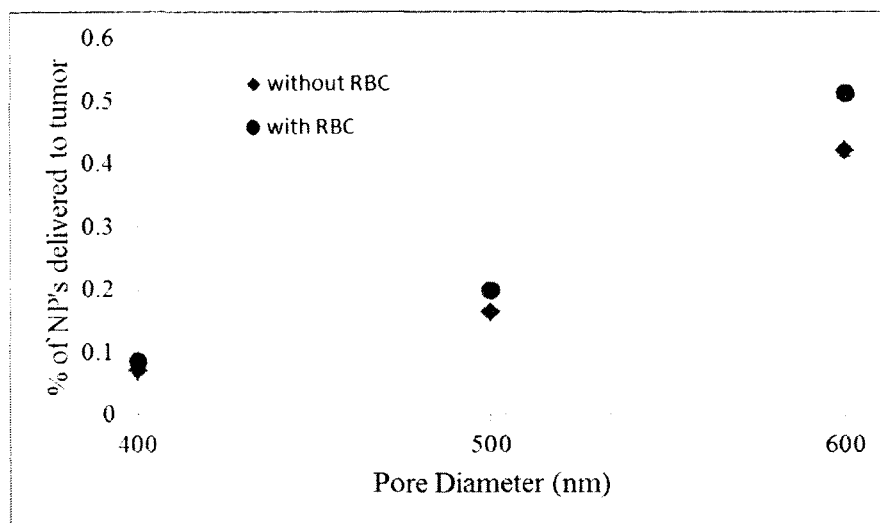


Figure 4.5: Comparison of NP's delivered to tumor with and without RBC in the capillary for different pore size

The NP diameter in these simulations is 200 nm. It can be observed from Figure 4.5 that the delivery to the tumor increased when RBC's are also simulated in the capillary; this is because the bolus flow of the plasma in between RBC's has radial velocity which pushes the NP's towards the capillary wall. A larger number of NP's at the capillary wall leads to an increase in the NP delivery to tumor. About a 22% increase in the NP delivery is observed for all the three pores.

4.5.2 Simulations as a Function of NP Size and Blood Pressure

Simulations were conducted to study the effect of the NP size and blood pressure on the NP delivery to the tumor in the presence of RBC for head and neck carcinoma (IFP 19 mmHg), metastatic melanoma (IFP 18 mmHg), and rectal carcinoma (IFP 15.3 mmHg). Figure 4.6 shows the NP delivery to the tumor as a function of the NP size.

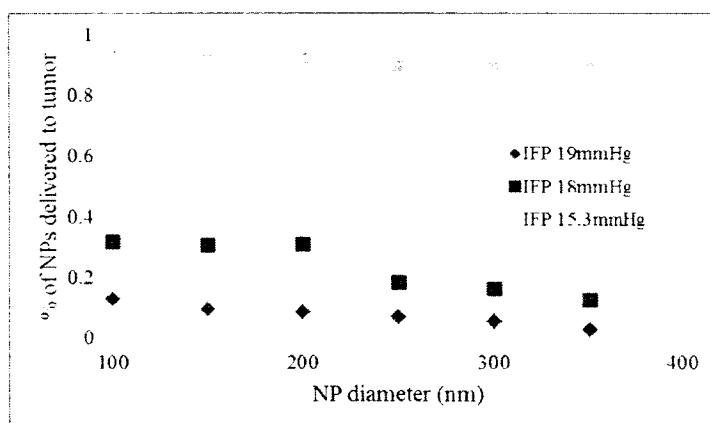


Figure 4.6: Percentage of NP's delivered to tumor as a function of NP size with RBC in the capillary

Capillary blood pressure in Figure 4.6 is 20 mmHg, and the pore diameter is 400 nm. It can be seen that the delivery of NP's behave in the same way as explained in Chapter 3 (Figure 3.3), i.e. for IFP 19 and 18, NP delivery decreases with an increase in its size but for tumors of IFP 15.3 mmHg, NP delivery is minimally affected by its size. Table 4.1 gives a comparison of the actual values of the % of NP's delivered for a 100 nm NP for various tumors with and without the presence of RBC.

Table 4.1: Comparison of the percentage of 100 nm NP delivered for different tumors with and without RBC in the capillary

IFP (mmHg)	% delivered for 100 nm NP with RBC	% delivered for 100 nm NP without RBC	% change
19	0.130 ± 0.004	0.100 ± 0.002	30%
18	0.320 ± 0.009	0.260 ± 0.007	23%
15.3	0.930 ± 0.014	0.760 ± 0.012	22%

From Table 4.1, it can be observed that the amount of NP's delivered increased in the presence of RBC in the capillary. Figure 4.7 shows the NP delivery as a function of the capillary blood pressure in the presence of RBC for different tumors.

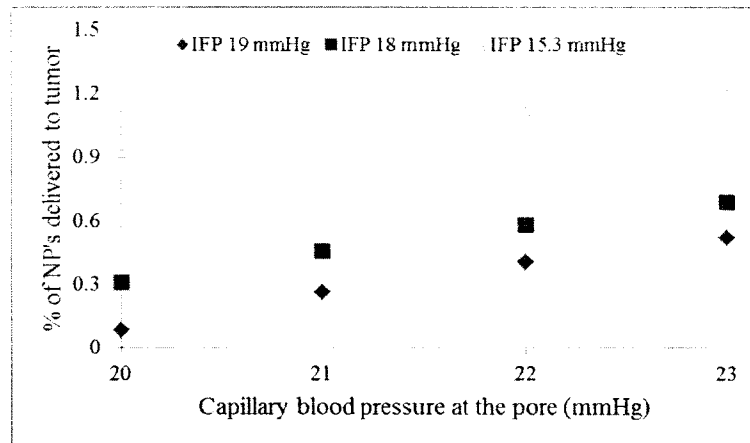


Figure 4.7: Percentage of NP's delivered to tumor as a function of capillary blood pressure in the presence of RBC in the capillary

NP and pore diameter in Figure 4.7 are 200 nm and 400 nm, respectively. Comparing these results to the results obtained in Figure 3.8 show that the NP delivery to the tumor increases approximately linearly with the increase in the blood pressure in both cases. Table 4.2 shows the % of NP's delivered to the tumor at a capillary blood pressure of 23 mmHg with and without RBC for all three different tumors.

Table 4.2: Percentage of NP's delivered to tumor at capillary blood pressure(CBP) 23 mmHg with and without RBC in the capillary

IFP (mmHg)	% of NP delivered for CBP 23mmHg with RBC	% of NP delivered for CBP 23mmHg without RBC	% change
19	0.520 ± 0.010	0.430 ± 0.006	21 %
18	0.690 ± 0.007	0.570 ± 0.009	21 %
15.3	1.210 ± 0.010	0.990 ± 0.009	22 %

It can be stated from these results that there is an increase in the amount of NP's delivered to the tumor in the presence of RBC in the capillary, but the delivery follows the same qualitative behavior as reported in Chapter 3.

CHAPTER 5

NANOPARTICLE FLOW THROUGH ENTIRE BODY

In this chapter, a study is performed in which the NP that flow through the entire body is considered and the NP delivery to the tumor through the capillary vessel is calculated with time and compared with the results of the PEG-liposomes and normal liposomes delivery obtained from an experimental group led by Ishida [133]. Unlike the previous chapters where NP flow through a section of the capillary is considered, this study considers the NP flow through an entire capillary vessel.

5.1 Number of Pores on the Capillary Wall

A study of the morphometric data on the endothelium of blood capillaries conducted by Simionescu and his group [134] infer that a single endothelial cell forms the cross-section of a visceral capillary and the width and length of an endothelial cell are 19.2 μm and 10 μm , respectively. The width of the endothelial cell forms the perimeter of the capillary cross section and its length adds up to the length of the capillary. According to this data, capillary of 700 μm length has 70 endothelial cells. Another experimental group led by Hashizume studied the number of pores in the capillaries and reported that 29% of the endothelial cells in a capillary wall form pores [135]. Utilizing their results, 29% of 70 cells, i.e. 20 cells, form pores, but since every two cells form a single pore, a total of 10 pores are present in a capillary.

5.2 Delivery through the Pores

Each pore is assumed to be present at a distance of $70\ \mu\text{m}$ from the adjacent pore such that a uniform distribution of pores on the capillary wall is obtained. The difference in the pressure at the arterial and venous end of the capillary is $20\ \text{mmHg}$ (Pressure values are obtained from Table 2.1) and the pressure drop for every $70\ \mu\text{m}$ distance in the capillary is $2\ \text{mmHg}$. Figure 5.1 shows the distribution of pores on the capillary wall and the blood pressure in the capillary at each pore.

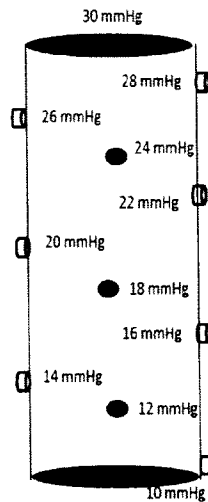


Figure 5.1: Distribution of pores and blood pressure in the capillary at each pore

Figure 5.2 shows the schematic of the drug transport in the capillary. As an example, the figure shows delivery through three pores considering the part of the capillary with each pore as a segment.

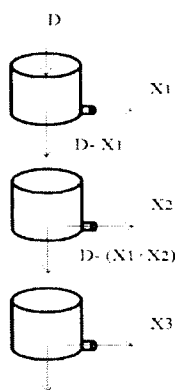


Figure 5.2: Schematic of the drug transport in the capillary

In Figure 5.2, D is the concentration of the drug in the blood flowing through the first segment of the capillary and X_1 is the amount of drug delivered to the tumor through pore one. As the blood enters the second segment, the drug dosage reduces to $D - X_1$, which means that as the blood passes through each pore, the dosage of drug reduces by the amount of drug delivered through that pore. The mean blood velocity in the capillary is 4.7 mm/s and hence the time needed for the blood to pass through a single pore is 0.015 seconds. Blood flow is continuous in the capillary and hence in 0.015 seconds, blood with dose D passes pore 1, blood with dose $D - X_1$ passes pore two, and so on. Hence, the drug delivered to the tumor in 0.015 seconds is the sum of the drug delivered through all five active pores in that time. The drug concentration in the first segment of the capillary is obtained as follows:

$$D = D_b \left(\frac{V_{bcs}}{V_{tb}} \right). \quad \text{Eq. 5.1}$$

where D_b is the drug dosage in the blood circulation, V_{bcs} is the Volume of the blood in the capillary segment, and V_{tb} is the total blood volume of the body.

The blood volume of a male mouse based on the experimental findings of Riches and his group is 84.7 ± 1.2 mL/Kg body weight [136] and hence the total blood volume in the male mouse used in the experiments of Ishida is 2.3 mL (Weight of the male mouse used in their experiments was 25-30 g).

In this study, delivery of a 100 nm NP (because average diameter of liposomes in the experiment was 100 nm) through head and neck carcinoma (IFP 19 mmHg) with tumor capillary pores of diameter 400 nm is studied. Delivery through each individual pore in the capillary is obtained by applying the results of the NP delivery through a single pore (from Chapter 3 and Chapter 4) for different capillary blood pressures simulated with the same pore diameter and for the same tumor as used in this study. Figure 5.3 shows the results for delivery of 100 nm NP through a pore diameter of 400 nm of head and neck carcinoma.

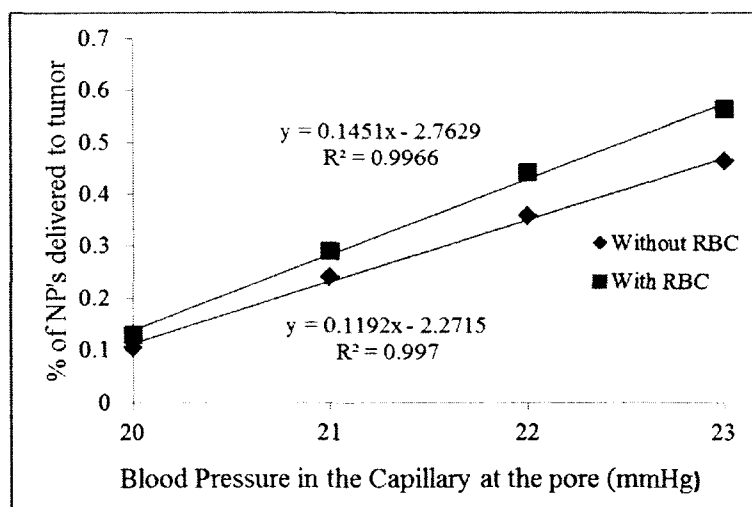


Figure 5.3: Delivery of NP's as a function of capillary blood pressure for 100 nm NP in head and neck carcinoma (IFP 19 mmHg)

Figure 5.3 is obtained from the results of Chapters 3 and 4. The figure shows that the delivery increases linearly with an increase in the blood pressure and the straight lines

which give the behavior of the drug delivery as a function of the blood pressure are extrapolated to get the delivery at capillary blood pressures 24, 26, and 28 mmHg. The % of NP's delivered obtained from extrapolation is shown in Figure 5.4.

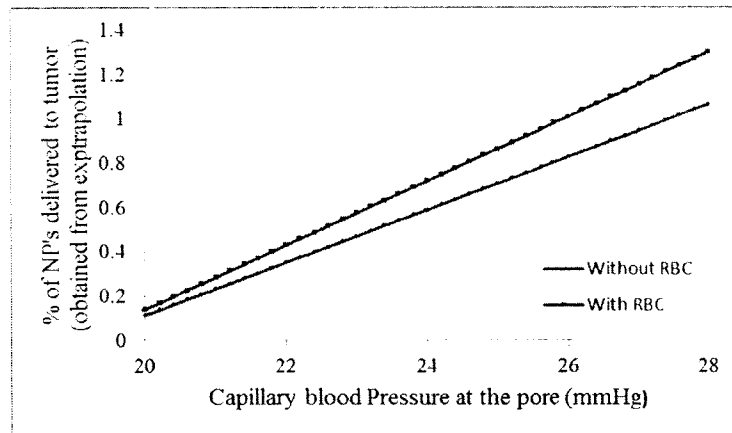


Figure 5.4: NP delivered to tumor obtained from extrapolation of results in chapter 3 and 4.

Interstitial pressure in this case (head and neck carcinoma) is 19 mmHg and, hence, for the highest blood pressure considered, i.e. for 28 mmHg, pressure difference across the pore is 9 mmHg. Figure 5.5 showing the percentage of NP's delivered to the tumor vs. pressure gradient across the capillary pore for rectal carcinoma (obtained from results of Chapters 3 and 4) states that even for a higher pressure gradient of 7.7 mmHg across the pore, the delivery is still linear and hence validates the linear extrapolation of the delivery rates shown in Figure 5.4.

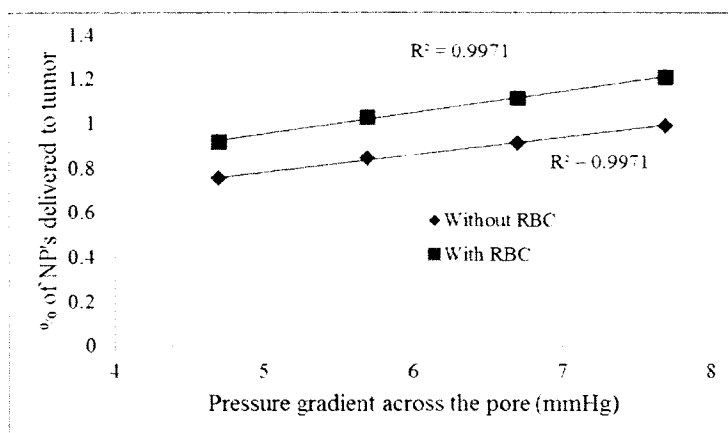


Figure 5.5: Delivery of NP's to tumor for different pressure gradients across the pore for 200 nm NP in rectal carcinoma (IFP 15.3 mmHg)

The NP diameter in Figure 5.5 is 200 nm and the pore diameter is 400 nm. For the pores with a capillary blood pressure less than 19 mmHg, there is a negative pressure gradient resulting in a flow from the tumor interstitium into the capillary. However, in this study we consider there is no flow of NP from the tumor to the capillary. This is because NP within the tumor interstitium travel through diffusion in all directions[137] leading to a lower fraction of NP's near these pores (within the interstitium), thereby causing a low or no re-entry of NPs from the interstitium to the capillary. Hence, in this study, pores with capillary blood pressure less than the tumor interstitial pressure are considered functionally inactive.

5.3 Drug Dosage in the Blood

Drug introduced into the body intravenously travel through the entire body and has an equal probability of entering the blood vessels of all body tissues. Hence, the drug in this study is considered to be uniformly distributed throughout the entire blood circulation such that at any given time, all blood vessels carry equal drug concentration.

In the experiments by Ishida (experiments with which this study is compared), an initial drug dosage of 500 μg is introduced into the body of a male mice [133]. As the drug circulates through the body, some part of it is accumulated in the liver and spleen and some part is delivered to the tumor, leading to a gradual decrease in the drug dosage in the blood with time. Experiments (by Ishida) were conducted for normal liposomes and PEG-liposomes with the same initial drug concentration, but the drug concentration remaining in the blood with time was observed to be different in each case as shown in Figure 5.6.

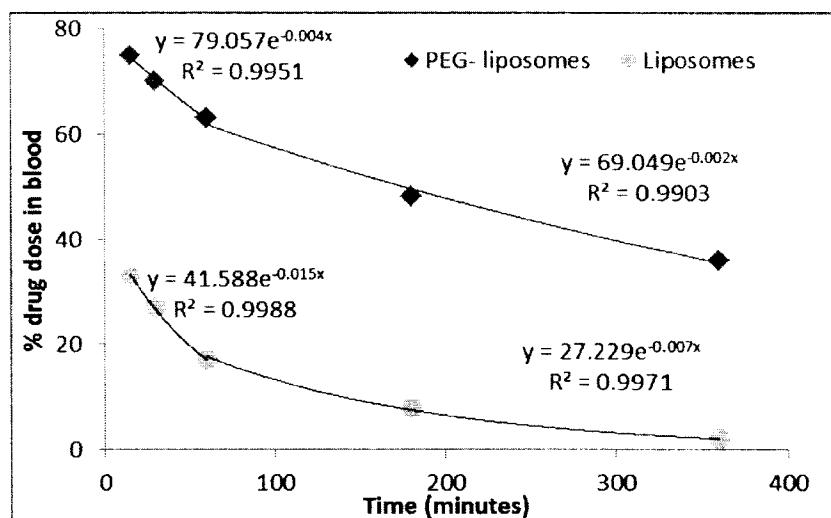


Figure 5.6: Percentage of drug dose remaining in the blood with time obtained from Ishida experiments [133]

In our study, the amount of drug remaining in the blood with time is obtained by using the exponential fits (black lines) from Figure 5.6 for liposomes and PEG-liposomes.

5.4 Results and Discussions

Delivery of normal liposomes and the PEG-liposomes (both liposomes have the same initial drug concentration but drug concentration remaining in the blood with time is different) to the tumor with time is calculated and compared to the experimental results obtained by Ishida as shown in Figure 5.7.

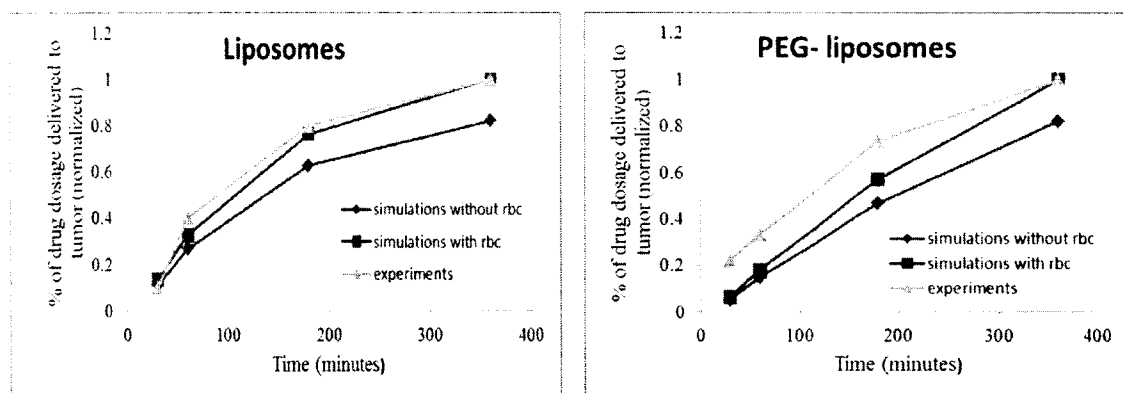


Figure 5.7: Experimental and simulated results of the delivery of liposomes to the tumor

In Figure 5.7 both the simulation results (with and without RBC) are normalized by the maximum drug delivery obtained in the presence of RBC after 360 minutes, whereas the experimental results are normalized by the drug delivery found in the tumor in experiments after 360 minutes. The actual percentage of drug delivered is shown in Table 5.1 for PEG-liposomes and Table 5.2 for normal liposomes.

Table 5.1: Actual percentage of drugs delivered in experiments and simulations for PEG-liposomes

Time (minutes)	PEG-liposomes (%)		
	Experiments	Simulations with RBC	Simulations without RBC
30	2.5	0.00024	0.00020
60	3.75	0.00067	0.00055
180	8.26	0.00210	0.00173
360	11.25	0.00370	0.00303

Table 5.2: Actual percentage of drugs delivered in experiments and simulations for liposomes

Time (minutes)	Liposomes (%)		
	Experiments	Simulations with RBC	Simulations without RBC
30	0.25	0.00010	0.00008
60	1	0.00024	0.00020
180	2	0.00056	0.00046
360	2.5	0.00073	0.00060

The actual delivery rates of the experiments are 10^3 times larger than the delivery rates from simulations; this is because in this study the blood flow through a single capillary of the tumor is considered, whereas in reality at any given point of time, blood simultaneously flows through a number of capillaries within the tumor tissue. Tumor tissue may contain thousands of capillaries and hence it is reasonable to have delivery

rates 10^3 times larger than the simulation results. Also, Figure 5.7 shows that the delivery behavior obtained from simulations agree with the delivery behavior of the experiments.

CHAPTER 6

CONCLUSIONS AND FUTURE WORK

6.1 Conclusions

1. A model to simulate the NP delivery to the tumor tissue through the tumor capillary wall pore was developed. The model uses a parametric equation to describe the particles flow in the capillary while a velocity profile predicted in COMSOL is utilized near the pore. Brownian motion is over imposed to the flow-induced particle transport. A uniform distribution of NP's in the capillary is achieved.
2. The effect of NP size, pore size, NP concentration, and capillary blood pressure on the delivery of NPs to different tumors such as head and neck carcinoma, metastatic melanoma and rectal carcinoma is studied.
3. A decrease in the delivery of NPs is observed with an increase in the NP size for head and neck carcinoma (IFP 19mmHg) and metastatic melanoma (IFP 18 mmHg), but for rectal carcinoma (IFP 15.3 mmHg), increase in the NP size did not affect the delivery by much.
4. An increase in the pore size increased the NP delivery to all three tumors. The results obtained for the effect of the NP size and pore size on the delivery made a qualitative agreement to the experimental results.

5. Increase in the NP concentration did not improve the efficiency of NP delivery to the tumor.
6. With the increase in the capillary blood pressure, the NP delivery to the tumor also increased.
7. The relative effect of IFP, capillary blood pressure, pore diameter, and particle size can be used to optimize the conditions for drug delivery. Pore size can be controlled by temperature [121], capillary blood pressure can be altered by administering vasoconstrictors to the body, and IFP can be controlled by using antiangiogenic agents [138].
8. Flow of RBC in the capillary is modeled. In this simulation it was ensured that the hematocrit is within physiological range. The bolus flow of plasma in the presence of RBC pushes the NP's towards the capillary wall leading to an increased NP delivery to the tumor; however, the behavior of the delivery as a function of NP size, blood pressure and interstitial fluid pressure does not change.
9. A study considering the drug flow through the entire body is performed. The drug concentration remaining in blood with time obtained from an experimental result by Ishida [133] is adopted into the study. The drug delivered to the tumor with time showed a very good agreement to the experimental results of Ishida.

6.2 Future Work

1. The model can be improved by finding an analytical solution for the flow of NP at the pore such that the model does not depend on COMSOL to get the velocity profile at the pore.

2. The model can be extended to include the transport of NP's in the tumor interstitium. The tumor interstitium is mainly composed of collagen and elastic fiber network with interstitial fluid in it [139]. The main transport of NP's through the tumor interstitium is through diffusion [137]. The transport of NP's in the interstitium can be modeled as diffusion through porous media to study how deep the NP can penetrate into the tumor. Also, the transport of NP's through the pore can be modeled.
3. Charge interactions between the NP and the capillary wall can be introduced into the model. Endothelial cells in the capillary walls are coated with glycocalyx, which has negatively charged sulphate and carboxylate groups, and the red blood cells also have a net negative charge on their surface [140]. Interactions between charged NP's, red blood cells and the glycocalyx can be modeled to study the delivery of a charged NP into the tumor interstitium.
4. The current model assumes that the NP's flow with the velocity of the blood. Drag forces of the blood flow acting on the nanoparticles can be included into the model to make it a more efficient model.

APPENDIX A

FLOW CHART OF THE PROGRAM

A.1. Flow Chart of the Program without RBC in Capillary

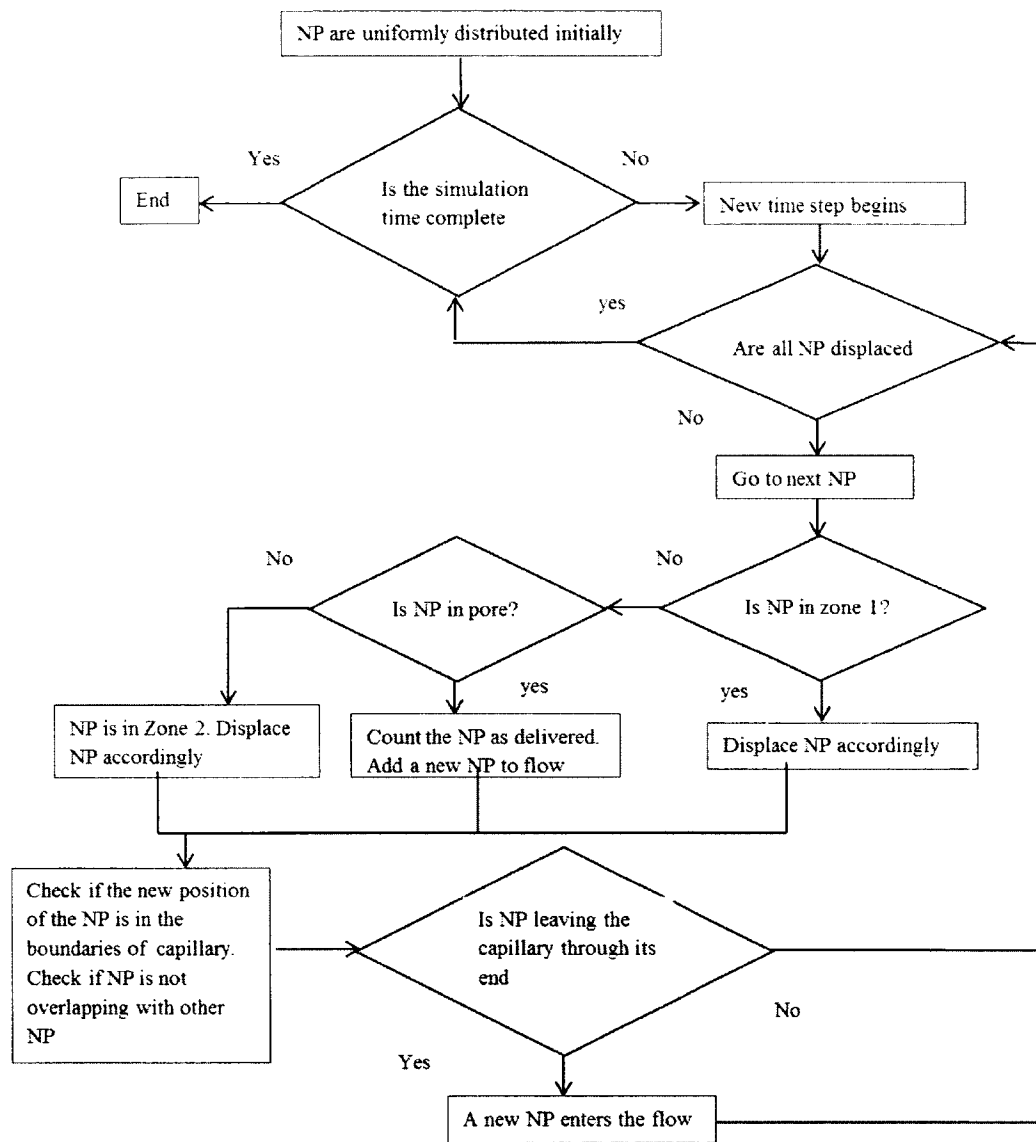


Figure A.1: Flow chart of the program without RBC in the capillary

A.2. Flow Chart of the Program with RBC in Capillary

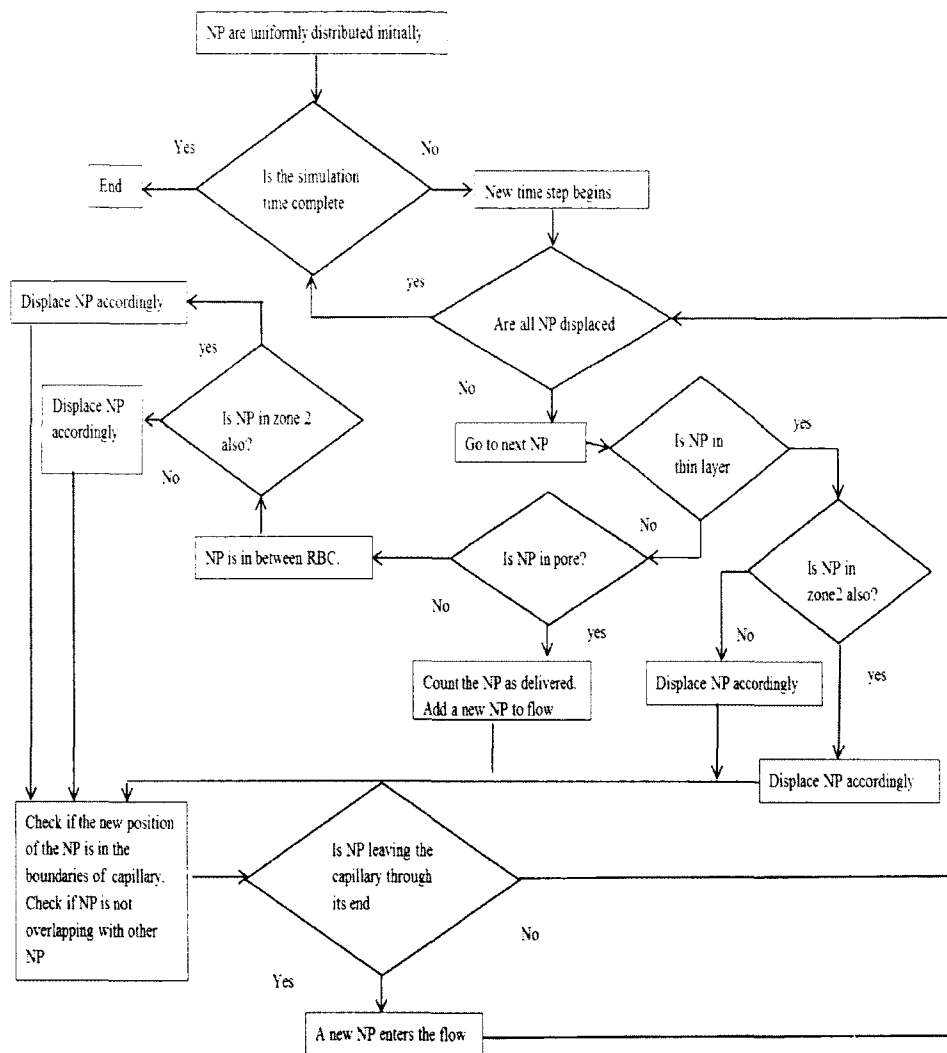


Figure A.2: Flow chart of program with RBC in capillary

APPENDIX B

VBA CODE FOR COMSOL DATA

B.1. Subtracting Velocity of Flow with and without Pore

Sub checkz()

Dim n As Integer, m As Integer, column1 As Integer, column2 As Integer, column3 As Integer, column4 As Integer, column5 As Integer

n = 2

m = 2

column1 = 3

column2 = 10

column3 = 6

column4 = 5

column5 = 11

Do While n < 33563

Do While (Abs(ActiveSheet.Cells(n, column1) - ActiveSheet.Cells(m, column2)) > 0.0009)

m = m + 1

Loop

ActiveSheet.Cells(n, column3) = ActiveSheet.Cells(n, column4) - ActiveSheet.Cells(m, column5)

n = n + 1

Loop

End Sub

B.2. Creating Co-ordinates of Velocity Table

```
Sub createpoint()
```

```
Dim x As Double, d As Double, z As Double, d1 As Double, y As Double, k As Integer, i
```

```
As Integer, j As Integer, l As Integer, column1 As Integer, column2 As Integer, column3
```

```
As Integer
```

```
x = 3.9265
```

```
d = 0.083 * 2
```

```
d1 = 0.2
```

```
l = 2
```

```
column1 = 8
```

```
column2 = 9
```

```
column3 = 10
```

```
For k = 1 To 10
```

```
z = 23.2
```

```
For i = 1 To 20
```

```
y = -2
```

```
For j = 1 To 20
```

```
ActiveSheet.Cells(l, column1) = x
```

```
ActiveSheet.Cells(l, column2) = y + d1
```

```
ActiveSheet.Cells(l, column3) = z
```

```
y = ActiveSheet.Cells(l, column2)
```

```
l = l + 1
```

```
Next j
z = z + dl
Next i
x = x - d
Next k
End Sub
```

B.3. Getting Velocities for the Table from COMSOL Data

```
Sub comparevz()
Dim n As Integer, m As Integer, column1 As Integer, column2 As Integer, column3 As
Integer, column4 As Integer, column5 As Integer, column6 As Integer, column8 As
Integer, column9 As Integer, column10 As Integer, column11 As Integer, column12 As
Integer, column13 As Integer, column14 As Integer, column15 As Integer, column16 As
Integer
m = 6
column1 = 1
column2 = 2
column3 = 3
column4 = 4
column5 = 5
column6 = 6
column8 = 8
column9 = 9
column10 = 10
```

```
column11 = 11
column12 = 12
column13 = 13
Do While m < 1602
n = 2
d1 = (ActiveSheet.Cells(n, column1) - ActiveSheet.Cells(m, column8)) ^ 2
d2 = (ActiveSheet.Cells(n, column2) - ActiveSheet.Cells(m, column9)) ^ 2
d3 = (ActiveSheet.Cells(n, column3) - ActiveSheet.Cells(m, column10)) ^ 2
Do While Sqr(d1 + d2 + d3) > 0.1
n = n + 1
d1 = (ActiveSheet.Cells(n, column1) - ActiveSheet.Cells(m, column8)) ^ 2
d2 = (ActiveSheet.Cells(n, column2) - ActiveSheet.Cells(m, column9)) ^ 2
d3 = (ActiveSheet.Cells(n, column3) - ActiveSheet.Cells(m, column10)) ^ 2
If n > 20008 Then Exit Do
Loop
If n < 20009 Then
ActiveSheet.Cells(m, column11) = ActiveSheet.Cells(n, column4)
ActiveSheet.Cells(m, column12) = ActiveSheet.Cells(n, column5)
ActiveSheet.Cells(m, column13) = ActiveSheet.Cells(n, column6)
Else
ActiveSheet.Cells(m, column11) = ActiveSheet.Cells(m - 1, column11)
ActiveSheet.Cells(m, column12) = ActiveSheet.Cells(m - 1, column12)
ActiveSheet.Cells(m, column13) = ActiveSheet.Cells(m - 1, column13)
```

```

End If
m = m + 1
Loop
End Sub

```

B.4. Finding the Highest Velocity in X, Y and Z Directions in Zone2

```

Sub checkhighvel()
Dim p As Double, n As Integer, m As Integer, column1 As Integer, column2 As Integer,
column3 As Integer, column4 As Integer
n = 1282
m = 2
p = 0.2
column1 = 3
column2 = 4
column3 = 15
column4 = 14
Do While n < 32002
Do While (ActiveSheet.Cells(n, column1) = p)
If Abs (ActiveSheet.Cells(n, column2)) > Abs(ActiveSheet.Cells(m, column3)) Then
ActiveSheet.Cells(m, column3) = ActiveSheet.Cells(n, column2)
End If
n = n + 1
Loop
ActiveSheet.Cells(m, column4) = p

```

p = p + 0.2

m = m + 1

Loop

End Sub

B.5. Comparing Velocities from Intrapolation and Table

Sub comparevz()

Dim n As Integer, m As Integer, column1 As Integer, column2 As Integer, column3 As Integer, column4 As Integer, column5 As Integer, column6 As Integer, column8 As Integer, column9 As Integer, column10 As Integer, column11 As Integer, column12 As Integer, column13 As Integer, column14 As Integer, column15 As Integer, column16 As Integer

m = 2

column1 = 1

column2 = 2

column3 = 3

column4 = 4

column5 = 5

column6 = 6

column8 = 8

column9 = 9

column10 = 10

column11 = 11

column12 = 12

```
column13 = 13
column14 = 14
column15 = 15
column16 = 16
Do While m < 1002
n = 2
d1 = (ActiveSheet.Cells(n, column1) - ActiveSheet.Cells(m, column8)) ^ 2
d2 = (ActiveSheet.Cells(n, column2) - ActiveSheet.Cells(m, column9)) ^ 2
d3 = (ActiveSheet.Cells(n, column3) - ActiveSheet.Cells(m, column10)) ^ 2
Do While Sqr(d1 + d2 + d3) > 0.05
n = n + 1
d1 = (ActiveSheet.Cells(n, column1) - ActiveSheet.Cells(m, column8)) ^ 2
d2 = (ActiveSheet.Cells(n, column2) - ActiveSheet.Cells(m, column9)) ^ 2
d3 = (ActiveSheet.Cells(n, column3) - ActiveSheet.Cells(m, column10)) ^ 2
If n > 4001 Then Exit Do
Loop
If n < 4002 Then
ActiveSheet.Cells(m, column14) = ActiveSheet.Cells(m, column11) -
ActiveSheet.Cells(n, column4)
ActiveSheet.Cells(m, column15) = ActiveSheet.Cells(m, column12) -
ActiveSheet.Cells(n, column5)
ActiveSheet.Cells(m, column16) = ActiveSheet.Cells(m, column13) -
ActiveSheet.Cells(n, column6)
```

End If

m = m + 1

Loop

End Sub

BIBLIOGRAPHY

- [1] J. Ferlay, *et al.* GLOBOCAN 2008 v2.0, Cancer Incidence and Mortality Worldwide: IARC CancerBase No. 10 [Online].
- [2] American Cancer Society. (2012, Oct. 10,). *Advanced Cancer*. Available: <http://www.cancer.org/acs/groups/cid/documents/webcontent/003082-pdf.pdf>.
- [3] J. A. Fidalgo, *et al.*, "Removal of primary tumor improves survival in metastatic breast cancer. Does timing of surgery influence outcomes," *Breast*, vol. 20, p. 7, 2011.
- [4] V. DeVita , *et al.*, *Cancer: Principles and Practice of Oncology*, 8th ed. Philadelphia: Lippincott Williams and Wilkins, 2008.
- [5] A. C. Society. (2011). *Understanding Chemotherapy: A Guide for Patients and Families*. Available: <http://www.cancer.org/acs/groups/cid/documents/webcontent/003025-pdf.pdf>.
- [6] A. Coates, *et al.*, "On the receiving end patient perception of the side-effects of cancer chemotherapy," *European Journal of Cancer and Clinical Oncology*, vol. 19, p. 6, 1983.
- [7] W. H. De Jong and P. J. Borm, "Drug delivery and nanoparticles: applications and hazards.," *Int J Nanomedicine*, vol. 3, p. 16, 2008.
- [8] J. Barichello, *et al.*, "Encapsulation of hydrophilic and lipophilic drugs in PLGA nanoparticles by the nanoprecipitation method.," *Drug Dev Ind Pharm*, vol. 25, p. 6, 1999.
- [9] L. Zhang, *et al.*, "Delivery of therapeutic radioisotopes using nanoparticle platforms: potential benefit in systemic radiation therapy," *Nanotechnology, Science and Applications*, vol. 3, p. 12, 2010.
- [10] J. M. Brown and A. J. Giaccia, "The Unique Physiology of Solid Tumors: Oppurtunities (and problems) for Cancer Therapy," *Cancer Res*, vol. 58, p. 9, 1998.
- [11] F. D. William and J. Folkman. (2008). *Angiogenesis: An Integrative Approach from Science to Medicine*.
- [12] G. Breier, "Angiogenesis in embryonic development--a review," *Placenta*, vol. 21 p. 7, 2000.

- [13] L. Shao and C. Zhu, "Angiogenesis in female reproductive system," *Chinese Science Bulletin*, vol. 46, p. 4, 2001.
- [14] F. Arnold and D. C. West, "Angiogenesis in wound healing," *Pharmacology & Therapeutics*, vol. 52, p. 16, 1991.
- [15] M. Klagsbrun and M. A. Moses, "Molecular angiogenesis," *Chemistry & Biology*, vol. 6, p. 8, 1999.
- [16] J. Folkman, "Clinical Applications of Research on Angiogenesis," *New England Journal of Medicine*, vol. 333, p. 7, 1995.
- [17] E. K. Rofstad and T. Danielsen, "Hypoxia-induced angiogenesis and vascular endothelial growth factor secretion in human melanoma," *Br J Cancer*, vol. 77, p. 6, 1998.
- [18] G. Bergers and L. E. Benjamin, "Tumorigenesis and the Angiogenic Switch," *Nature Reviews Cancer*, vol. 3, p. 10, 2003.
- [19] I. Kim, *et al.*, "Angiopoietin-1 Reduces VEGF-Stimulated Leukocyte Adhesion to Endothelial Cells by Reducing ICAM-1, VCAM-1, and E-Selectin Expression," *Circulation Research*, vol. 89, p. 3, 2001.
- [20] C. Suri, *et al.*, "Requisite Role of Angiopoietin-1, a Ligand for the TIE2 Receptor, during Embryonic Angiogenesis," *Cell*, vol. 87, p. 10, 1996.
- [21] R. E. Friesel and T. Maciag, "Molecular mechanisms of angiogenesis: fibroblast growth factor signal transduction," *The FASEB Journal*, vol. 9, p. 7, 1995.
- [22] G. A. Truskey, *Transport phenomenon in biological systems*, 2nd edition ed.: Prentice Hall, 2004.
- [23] J. E. H. Arthur C. Guyton. (2005). *Textbook of Medical Physiology (11 ed.)*.
- [24] B. M. van den Berg, *et al.*, "The Endothelial Glycocalyx Protects Against Myocardial Edema," *Circulation Research*, vol. 92, p. 3, 2003.
- [25] M. Gouverneur, *et al.*, "Fluid shear stress stimulates incorporation of hyaluronan into endothelial cell glycocalyx," *American Journal of Physiology - Heart and Circulatory Physiology*, vol. 290, p. 7, 2006.
- [26] V. S. LeBleu, *et al.*, "Structure and Function of Basement Membranes," *Experimental Biology and Medicine*, vol. 232, p. 9, 2007.
- [27] S. C. Satchell and F. Braet, "Glomerular endothelial cell fenestrations: an integral component of the glomerular filtration barrier," *American Journal of Physiology - Renal Physiology*, vol. 296, p. 10, 2009.

- [28] R. H. Thomlinson and L. H. Gray, "The Histological Structure of Some Human Lung Cancers and the Possible Implications for Radiotherapy," *Br J Cancer*, vol. 9, p. 11, 1955.
- [29] T. G. Simonsen, *et al.*, "High Interstitial Fluid Pressure Is Associated with Tumor-Line Specific Vascular Abnormalities in Human Melanoma Xenografts," *PLoS ONE*, vol. 7, p. 7, 2012.
- [30] C. H. Heldin, *et al.*, "High interstitial fluid pressure : an obstacle in cancer therapy," *Nat Rev Cancer*, vol. 4, p. 8, 2004.
- [31] K. Alitalo and P. Carmeliet, "Molecular mechanisms of lymphangiogenesis in health and disease," *Cancer cell*, vol. 1, p. 9, 2002.
- [32] T. P. Padera, *et al.*, "Lymphatic Metastasis in the Absence of Functional Intratumor Lymphatics," *Science*, vol. 296, p. 4, 2002.
- [33] A. J. Leu, *et al.*, "Absence of functional lymphatics within a murine sarcoma: a molecular and functional evaluation," *Cancer Res*, vol. 60, p. 4, 2000.
- [34] *Understanding Cancer Series*. Available: <http://www.cancer.gov/cancertopics/understandingcancer/cancer/AllPages>.
- [35] *What are Carcinomas?* Available: <http://www.news-medical.net/health/What-are-Carcinomas.aspx>.
- [36] *Overview of Epithelial Cells*. Available: <http://www.bio.davidson.edu/people/kabernd/BerndCV/Lab/EpithelialInfoWeb/index.html>.
- [37] *Sarcoma Alliance*. Available: <http://sarcomaalliance.org/what-you-need-to-know/what-is-sarcoma>.
- [38] *Sarcoma- Adult Soft Tissue Cancer*. Available: <http://www.cancer.org/cancer/sarcoma-adultsofttissuecancer/detailedguide/sarcoma-adult-soft-tissue-cancer-soft-tissue-sarcoma>.
- [39] *What is Lymphoma?* Available: <http://americancancerfund.org/facts-about-cancer/basic-info/lymphoma>.
- [40] *Lymphoma Info*. Available: <http://www.lymphomainfo.net/lymphoma/whatis.html>.
- [41] *Childhood Leukemia*. Available: <http://www.cancer.org/cancer/leukemiachildren/detailedguide/childhood-leukemia-what-is-childhood-leukemia>.

- [42] B. A. Bornstein, *et al.*, "Results of treating ductal carcinoma In situ of the breast with conservative surgery and radiation therapy," *Cancer*, vol. 67, p. 7, 1991.
- [43] Z. J. Xia, *et al.*, "Phase III randomized clinical trial of intratumoral injection of E1B gene-deleted adenovirus (H101) combined with cisplatin-based chemotherapy in treating squamous cell cancer of head and neck or esophagus," *Ai zheng Chinese journal of cancer*, vol. 23, p. 5, 2004.
- [44] Z. Hu and A. Garen, "Targeting tissue factor on tumor vascular endothelial cells and tumor cells for immunotherapy in mouse models of prostatic cancer," *Proceedings of the National Academy of Sciences*, vol. 98, p. 6, 2001.
- [45] "Cancer Treatment and Survivorship Facts & Figures 2012-2013," *American Cancer Society*.
- [46] J. D. F. Allendorf, *et al.*, "Tumor growth after laparotomy or laparoscopy," *Surgical Endoscopy*, vol. 9, p. 4, 1995.
- [47] G. H. Bruce and D. W. Lynn, *Handbook of Radiation Oncology: Basic Principles and Clinical Protocols*, 1st ed.: Jones and Bartlett Publishers, 2008.
- [48] R. R. Patel and D. W. Arthur, "The Emergence of Advanced Brachytherapy Techniques for Common Malignancies," *Hematology/oncology clinics of North America*, vol. 20, p. 21, 2006.
- [49] D. Peer, *et al.*, "Nanocarriers as an emerging platform for cancer therapy," *Nat Nano*, vol. 2, p. 10, 2007.
- [50] J. E. Groopman and L. M. Itri, "Chemotherapy-Induced Anemia in Adults: Incidence and Treatment," *Journal of the National Cancer Institute*, vol. 91, p. 19, 1999.
- [51] T. A. Waldmann, "Immunotherapy: Past, Present and Future," *Nat Med*, vol. 9, p. 9, 2003.
- [52] M. Dougan and G. Dranoff, "Immunotherapy of Cancer: Innate Immune Regulation and Cancer Immunotherapy," R. Wang, Ed., ed: Springer New York, 2012.
- [53] O. Al-Mefty, *et al.*, "The long-term side effects of radiation therapy for benign brain tumors in adults," *Journal of Neurosurgery*, vol. 73, p. 11, 1990.
- [54] S. Mitra, *et al.*, "Tumour targeted delivery of encapsulated dextran–doxorubicin conjugate using chitosan nanoparticles as carrier," *Journal of Controlled Release*, vol. 74, p. 7, 2001.

- [55] K. Kairemo, *et al.*, "Nanoparticles in Cancer," *Current Radiopharmaceuticals*, vol. 1, p. 7, 2008.
- [56] L. Jing and G. Min, "Gold-Nanoparticle-Enhanced Cancer Photothermal Therapy," *Selected Topics in Quantum Electronics, IEEE Journal of*, vol. 16, p. 8, 2010.
- [57] W. J. Gradishar, *et al.*, "Phase III Trial of Nanoparticle Albumin-Bound Paclitaxel Compared With Polyethylated Castor Oil–Based Paclitaxel in Women With Breast Cancer," *Journal of Clinical Oncology*, vol. 23, p. 10, 2005.
- [58] C. Li, "Poly(l-glutamic acid)–anticancer drug conjugates," *Advanced Drug Delivery Reviews*, vol. 54, p. 18, 2002.
- [59] M. L. Adams, *et al.*, "Amphiphilic block copolymers for drug delivery," *Journal of Pharmaceutical Sciences*, vol. 92, p. 13, 2003.
- [60] S. F. Svenson and D. A. Tomalia, "Dendrimers in biomedical applications--reflections on the field," *Adv Drug Deliv Rev*, vol. 57, p. 23, 2005.
- [61] C. J. Hu, *et al.*, "Nanoparticle-assisted combination therapies for effective cancer treatment," *Therapeutic Delivery*, vol. 1, p. 12, 2010.
- [62] K. Cho, *et al.*, "Therapeutic Nanoparticles for Drug Delivery in Cancer," *Clinical Cancer Research*, vol. 14, p. 7, 2008.
- [63] L. F. Zhang, *et al.*, "Development of nanoparticles for antimicrobial drug delivery," *Curr Med Chem*, vol. 17, p. 10, 2010.
- [64] M. Markman, "Pegylated liposomal doxorubicin in the treatment of cancers of the breast and ovary," *Expert Opin Pharmacother*, vol. 7, p. 6, 2006.
- [65] E. Rivera, "Current status of liposomal anthracycline therapy in metastatic breast cancer," *Clin Breast Cancer*, vol. 4, p. 8, 2003.
- [66] P. F. Couvreur and C. Vauthier, "Nanotechnology: intelligent design to treat complex disease," *Pharm Res*, vol. 23, p. 35, 2006.
- [67] *Viral Nanoparticles*. Available: http://dujs.dartmouth.edu/wp-content/uploads/2011/03/6_pdfsam_11w_final.pdf.
- [68] K. L. Robertson and J. L. Liu, "Engineered viral nanoparticles for flow cytometry and fluorescence microscopy applications," *Wiley Interdisciplinary Reviews: Nanomedicine and Nanobiotechnology*, vol. 4, p. 14, 2012.
- [69] A. Bianco, *et al.*, "Applications of carbon nanotubes in drug delivery," *Current Opinion in Chemical Biology*, vol. 9, p. 6, 2005.

- [70] W. Cai, *et al.*, "Applications of gold nanoparticles in cancer nanotechnology," *Nanotechnology, Science and Applications*, vol. 1, p. 16, 2008.
- [71] X. F. Huang, *et al.*, "Plasmonic photothermal therapy (PPTT) using gold nanoparticles," *Lasers Med Sci*, vol. 23, p. 10, 2008.
- [72] S. J. Oldenburg, *et al.*, "Surface enhanced Raman scattering in the near infrared using metal nanoshell substrates," *J Chem Phys*, vol. 111, p. 7, 1999.
- [73] S. Link and M. A. El-Sayed, "Spectral Properties and Relaxation Dynamics of Surface Plasmon Electronic Oscillations in Gold and Silver Nanodots and Nanorods," *The Journal of Physical Chemistry B*, vol. 103, p. 17, 1999.
- [74] S. M. Moghimi, *et al.*, "Long-Circulating and Target-Specific Nanoparticles: Theory to Practice," *Pharmacological Reviews*, vol. 53, p. 35, 2001.
- [75] J. F. Jokerst, *et al.*, "Nanoparticle PEGylation for imaging and therapy," *Nanomedicine (Lond)*, vol. 6, p. 14, 2011.
- [76] *What Is the Reticuloendothelial System*. Available: <http://www.wisegeek.com/what-is-the-reticuloendothelial-system.htm>.
- [77] E. Sadauskas, *et al.*, "Protracted elimination of gold nanoparticles from mouse liver," *Nanomedicine: Nanotechnology, Biology, and Medicine*, vol. 5, p. 8, 2009.
- [78] G. Prencipe, *et al.*, "PEG Branched Polymer for Functionalization of Nanomaterials with Ultralong Blood Circulation," *Journal of the American Chemical Society*, vol. 131, p. 5, 2009.
- [79] G. S. Kwon, "Polymeric micelles for delivery of poorly water-soluble compounds," *Crit Rev Ther Drug Carrier Syst*, vol. 20, p. 20, 2004.
- [80] B. S. Zolnik and N. Sadrieh, "Regulatory perspective on the importance of ADME assessment of nanoscale material containing drugs," *Advanced Drug Delivery Reviews*, vol. 61, p. 6, 2009.
- [81] S. K. Hobbs, *et al.*, "Regulation of transport pathways in tumor vessels: Role of tumor type and microenvironment," *Proceedings of the National Academy of Sciences*, vol. 95, pp. 4607-4612, 1998.
- [82] F. Yuan, *et al.*, "Vascular Permeability in a Human Tumor Xenograft: Molecular Size Dependence and Cutoff Size," *Cancer Res*, vol. 55, p. 5, 1995.
- [83] R. A. Hannon, *et al.*, *Port Pathophysiology: Concepts of Altered Health States*, 2009.

- [84] R. F. Scow, *et al.*, "Transport of lipid across capillary endothelium," *Fed Proc*, vol. 39, p. 7, 1980.
- [85] M. Bundgaard, "The three-dimensional organization of tight junctions in a capillary endothelium revealed by serial-section electron microscopy," *J Ultrastruct Res*, vol. 88, p. 17, 1984.
- [86] M. J. Karnovsky, "The ultrastructural basis of capillary permeability studied with peroxidase as a tracer," *J Cell Biol*, vol. 35, p. 23, 1968.
- [87] S. F. Wissig and M. C. Williams, "Permeability of muscle capillaries to microperoxidase," *J Cell Biol*, vol. 76, p. 20, 2000.
- [88] A. F. Milici, *et al.*, "Transcytosis of albumin in capillary endothelium," *J Cell Biol*, vol. 105, p. 10, 1988.
- [89] *Human Cardiac Anatomy*. Available: <http://www.vhlab.umn.edu/atlas/physiology-tutorial/blood-vessels.shtml>.
- [90] *In Cell Biology, What are Vesicles*. Available: <http://www.wisegeek.com/in-cell-biology-what-are-vesicles.htm>.
- [91] C. C. Michel, "Transport of macromolecules through microvascular walls," *Physiol Rev*, vol. 74, p. 26, 1996.
- [92] D. F. Predescu, *et al.*, "Binding and transcytosis of glycoalbumin by the microvascular endothelium of the murine myocardium: evidence that glycoalbumin behaves as a bifunctional ligand," *J Cell Biol*, vol. 107, p. 10, 1988.
- [93] W. A. Jefferies, *et al.*, "Transferrin receptor on endothelium of brain capillaries," *Nature*, vol. 312, p. 2, 1984.
- [94] G. F. King and S. M. Johnson, "Receptor-mediated transport of insulin across endothelial cells," *Science*, vol. 227, p. 4, 1985.
- [95] M. F. Tavassoli, *et al.*, "Liver endothelium mediates the hepatocyte's uptake of ceruloplasmin," *J Cell Biol*, vol. 102, p. 5, 1986.
- [96] J. Zhang, *et al.*, "Design of Nanoparticles as Drug Carriers for Cancer Therapy," *Cancer Genomics - Proteomics*, vol. 3, p. 10, 2006.
- [97] B. Haraldsson, "Physiological studies of macromolecular transport across capillary walls. Studies on continuous capillaries in rat skeletal muscle," *Acta Physiol Scand Suppl*, vol. 553, p. 40, 1987.
- [98] T. F. Koklic and J. Trancar, "Lysolipid containing liposomes for transendothelial drug delivery," *BMC Res Notes*, vol. 5, p. 8, 2012.

- [99] A. F. Orthmann, *et al.*, "Impact of membrane properties on uptake and transcytosis of colloidal nanocarriers across an epithelial cell barrier model," *J Pharm Sci*, vol. 99, p. 11, 2010.
- [100] P. Tartaj, *et al.*, "The preparation of magnetic nanoparticles for applications in biomedicine," *Journal of Physics D: Applied Physics*, vol. 36, p. 7, 2003.
- [101] B. S. Kuszyk, *et al.*, "Tumor Transport Physiology," *American Journal of Roentgenology*, vol. 177, p. 7, 2001.
- [102] R. K. Jain, "Barriers to drug delivery in solid tumors," *Sci Am*, vol. 271, p. 8, 1994.
- [103] R. K. Jain, "Transport of Molecules in the Tumor Interstitium: A Review," *Cancer Res*, vol. 47, p. 13, 1987.
- [104] V. Torchilin, "Antibody-modified liposomes for cancer chemotherapy," *Expert Opin Drug Deliv*, vol. 5, p. 22, 2008.
- [105] D. Kim, *et al.*, "A Drug-Loaded Aptamer–Gold Nanoparticle Bioconjugate for Combined CT Imaging and Therapy of Prostate Cancer," *ACS Nano*, vol. 4, p. 8, 2010.
- [106] D.-K. Chang, *et al.*, "A Novel Peptide Enhances Therapeutic Efficacy of Liposomal Anti-Cancer Drugs in Mice Models of Human Lung Cancer," *PLoS ONE*, vol. 4, p. 7, 2009.
- [107] C. Pozrikidis and D. A. Farrow, "A Model of Fluid Flow in Solid Tumors," *Annals of Biomedical Engineering*, vol. 31, p. 14, 2003.
- [108] M. Soltani and P. Chen, "Numerical Modeling of Fluid Flow in Solid Tumors," *PLoS ONE*, vol. 6, p. 7, 2011.
- [109] Chang, *et al.*, "Application of the network model for studying the delivery of colloidal drugs," *Colloid Polym Sci*, vol. 289, p. 14, 2011.
- [110] Mathworks, "MATLAB," R2011b ed, 2011.
- [111] P. Morters and Y. Peres. (2008). *Brownian Motion*.
- [112] N. C. Staub and E. L. Schultz, "Pulmonary capillary length in dog, cat and rabbit," *Respiration Physiology*, vol. 5, p. 9, 1968.
- [113] *Blood: composition and functions*. Available: http://simscience.org/membranes/advanced/essay/blood_comp_and_func1.html.
- [114] A. Y. Wonder, *Blood Dynamics*: Academic Press, 2001.

- [115] M. A. Rao, *Rheology of Fluid and Semisolid Foods: Principles and Applications*: Aspen Publ, 1999.
- [116] S. S. Shibeshi and W. E. Collins, "The Rheology of Blood Flow in a Branched Arterial System," *Appl Rheol*, vol. 15, p. 8, 2005.
- [117] COMSOL, "COMSOL Multiphysics," 4.0a ed. 2010.
- [118] *COMSOL MULTIPHYSICS*. Available: www.comsol.com.
- [119] J. D. Cutnell and K. W. Johnson, *Physics*, 4th ed., 1997.
- [120] R. K. Jain, *et al.*, "Effect of vascular normalization by antiangiogenic therapy on interstitial hypertension, peritumor edema, and lymphatic metastasis: insights from a mathematical model," *Cancer Res*, vol. 67, p. 7, 2007.
- [121] G. Kong, *et al.*, "Hyperthermia Enables Tumor-specific Nanoparticle Delivery: Effect of Particle Size," *Cancer Research*, vol. 60, p. 6, 2000.
- [122] i. A. F. Milic, *et al.*, "Transcytosis of albumin in capillary endothelium," *J Cell Biol*, vol. 105, p. 10, 1988.
- [123] K. Boryczko, *et al.*, "Dynamical clustering of red blood cells in capillary vessels," *J Mol Model*, vol. 9, p. 18, 2003.
- [124] Y. Liu and W. K. Liu, "Rheology of red blood cell aggregation by computer simulation," *J. Comput. Phys.*, vol. 220, p. 16, 2006.
- [125] C. F. McLaren, *et al.*, "Statistical and graphical evaluation of erythrocyte volume distributions," *Am J Physiol*, vol. 252, p. 10, 1987.
- [126] H. Sakai, *et al.*, "Peculiar flow patterns of RBCs suspended in viscous fluids and perfused through a narrow tube (25 μm)," *American Journal of Physiology - Heart and Circulatory Physiology*, vol. 297, p. 6, 2009.
- [127] K. H. Albrecht, *et al.*, "The Fahraeus effect in narrow capillaries (i.d. 3.3 to 11.0 μm)," *Microvascular Research*, vol. 18, p. 15, 1979.
- [128] T. F. Secomb, *et al.*, "Motion of red blood cells in a capillary with an endothelial surface layer: effect of flow velocity," *Am J Physiol Heart Circ Physiol*, vol. 281, p. 8, 2001.
- [129] Z. Y. Yan, "The "bolus flow" solution of the plasma between the red blood cells flowing through a capillary," *Sci Sin*, vol. 24, p. 13, 1982.
- [130] T. W. Secomb, *et al.*, "Tribology of capillary flow," *Proceedings of the Institution of Mechanical Engineers Part N Journal of Nanoengineering and Nanosystems*, vol. 220, p. 6, 2006.

- [131] G. Elert. *The Physics Hypertextbook*.
- [132] Y. C. Fung, "Blood Flow in the Capillary Bed," *J Biomechanics*, vol. 2, p. 20, 1969.
- [133] O. F. Ishida, *et al.*, "Size-dependent extravasation and interstitial localization of polyethyleneglycol liposomes in solid tumor-bearing mice," *Int J Pharm*, vol. 1999, p. 8, 1999.
- [134] M. F. Simionescu and G. E. Palade, "Morphometric data on the endothelium of blood capillaries," *J Cell Biol*, vol. 60, p. 25, 1974.
- [135] H. Hashizume, *et al.*, "Openings between defective endothelial cells explain tumor vessel leakiness," *Am J Pathol*, vol. 156, p. 17, 2006.
- [136] A. C. Riches, *et al.*, "Blood volume determination in the mouse," *J Physiol*, p. 6, 1973.
- [137] R. K. Jain and T. Stylianopoulos, "Delivering Nanomedicine to Solid Tumors," *Nat Rev Clin Oncol*, vol. 7, p. 2, 2010.
- [138] R. K. Jain, *et al.*, "Effect of vascular normalization by antiangiogenic therapy on interstitial hypertension, peritumor edema, and lymphatic metastasis: insights from a mathematical model.," *Cancer Res*, vol. 67, p. 7, 2007.
- [139] R. K. Jain, "Transport of Molecules in the Tumor Interstitium: A Review," *Cancer Research*, vol. 47, p. 13, 1987.
- [140] H. Vink, *et al.*, "Evidence that cell surface charge reduction modifies capillary red cell velocity-flux relationships in hamster cremaster muscle," *Journal of Physiology*, vol. 489, p. 9, 1995.